Real-Time Nerve Stimulation Artifact Removal for an Embedded Prosthesis Controller

Master's Thesis in Engineering Mathematics and Computational Science

ANTON BERNEVING

DEPARTMENT OF ELECTRICAL ENGINEERING

CHALMERS UNIVERSITY OF TECHNOLOGY
Gothenburg, Sweden 2021
www.chalmers.se

Master's thesis

Real-Time Nerve Stimulation Artifact Removal for an Embedded Prosthesis Controller

ANTON BERNEVING

Department of Electrical Engineering
CHALMERS UNIVERSITY OF TECHNOLOGY
Gothenburg, Sweden 2021

Real-Time Nerve Stimulation Artifact Removal for an Embedded Prosthesis Controller
ANTON BERNEVING

Masters Thesis in Engineering Mathematics and Computational Science
Department of Electrical Engineering
Chalmers University of Technology
SE-412 96 Göteborg
Sweden
Telephone +46 (0)31-772 1000

Cover: Manually activating the sensor on a prosthetic hand to produce sensory feedback for the prosthesis user.

Typeset in LaTeX
Printed by Chalmers Reproservice
Gothenburg, Sweden 2021

Real-Time Nerve Stimulation Artifact Removal for an Embedded Prosthesis Controller

ANTON BERNEVING
Department of Electrical Engineering
Chalmers University of Technology

Abstract

As the demand for prosthetic replacement devices with reliable and multi-functional control increases, recent advances in osseointegration, Targeted Muscle Reinnervation (TMR) and myoelectric pattern recognition have proven considerably advantageous. Using implanted electrodes around residual nerves, tactile feedback from the prosthetic device can also be achieved by neurostimulation. However, this stimulation causes interfering artifacts on the electromyogram (EMG) electrodes which affect reliability and function of the prosthesis device. Previous work on stimulation artifact removal has focused on using surface electrodes and other types of biosignals while leaving out the control aspect. Therefore, this thesis implements two real-time stimulation artifact removal algorithms and investigates their performance in relation to four signal features commonly used for myoelectric pattern recognition.

Signals containing stimulation artifacts and muscle EMG activity were recorded and analyzed offline to determine the artifact influence and to what extent the effects can be mitigated by the algorithms. Using semi-synthetic signals, sensitivity to variations in hyperparameters was also evaluated. To verify their real-time capability, the algorithms were implemented on an embedded prosthesis controller.

Visual inspection of feature value distributions indicate that the algorithms can reduce the effect of the stimulation artifacts, especially for Mean Absolute Value (MAV). Large performance variance between electrodes suggest that the artifact influence largely depends on recording electrode placement in relation to the stimulation electrode, and that factors such as signal strength and artifact amplitude need to be considered when choosing suitable algorithm hyperparameters. A preliminary online experiment provide similar observations, suggesting the algorithms' feasibility for usage in real-time on an embedded prosthesis controller.

Keywords: Artifact removal, Embedded device, Myoelectric prosthesis control, Sensory feedback

Acknowledgments

I would like to express my deepest gratitude to my supervisor Eric J. Earley for his never ending support, advice and feedback throughout the project. I must also thank Jan Zbinden for providing invaluable insights during our discussions, sharing his experience, and for his assistance during participant visits.

My gratitude is also extended to my examiner Max J. Ortiz-Catalán and to all members of the Center for Bionics and Pain Research (CBPR) for their warm welcome and support.

Finally, I would like to express my gratitude to my family and friends for their never ending love and encouragement.

Anton Berneving, Gothenburg, June 2021

Acronyms

ADC	Analog-to-Digital Converter
AR	autoregressive
BSS	Blind Source Separation
CCA	Canonical Correlation Analysis
DWT	Discrete Wavelet Transform
ECG	electrocardiogram
EEG	electroencephalogram
EMD	Empirical Mode Decomposition
EMG	electromyogram
FIR	Finite Impulse Response
ICA	Independent Component Analysis
IIR	Infinite Impulse Response
LDA	Linear Discriminant Analysis
LMS	Least Mean Squares
MAV	Mean Absolute Value
MCU	Microcontroller Unit
MINLP	Mixed-Integer Nonlinear Programming
MLP	multilayer perceptron
MSE	Mean Squared Error
MUAP	Motor Unit Action Potential
NLMS	Normalized Least Mean Squares
ϵ-NLMS	ϵ-Normalized Least Mean Squares
RLS	Recursive Least Squares
RMSE	Root Mean Squared Error
sEMG	surface electromyogram
SNR	Signal-to-Noise Ratio
SSC	Slope Sign Changes
SVN	Support Vector Machine
TMR	Targeted Muscle Reinnervation
TS	Template Subtraction
WL	Waveform Length
WT	Wavelet Transform
ZC	Zero Crossings

Contents

1

Introduction

In 2008, Ziegler-Graham *et al.* estimated that the number of people living with amputations in the US would more than double by the year 2050 [1]. Furthermore, it is estimated that there are more than 1 million annual limb amputations globally [2]. This poses a significant challenge as the demand for prosthetic replacement devices with reliable and multi-functional control for intuitive use in daily life increases.

During the last decades, most of the development has lead in the direction of introducing powered prostheses where movement control is decoded from surface electromyogram (sEMG) using myoelectric pattern recognition [3]. Further work has also been performed to improve control resolution and reliability through Targeted Muscle Reinnervation (TMR), where nerves in the remaining limb are innervated into existing musculature to increase the number of electromyogram (EMG) channels and improve prosthesis controllability [4].

However, using sEMG for prosthesis control comes with a multitude of problems as the signal quality is heavily dependent on environmental conditions and susceptible to motion artifacts and myoelectric crosstalk [5]. To remedy this, recent work extending the concept of bone-anchored (osseointegrated) prostheses to also include bi-directional electrical communication through the e-OPRA system [6] has allowed electrodes to be implanted and connected directly through the abutment to the prosthesis. This has improved controllability and general prosthesis usability over classical sEMG prostheses [5], [7], [8].

The bi-directional communication additionally allows neurostimulation to be used to provide feedback to the prosthesis user [5]. By placing spiral cuff electrodes around nerves in the residual limb, somatosensory (touch) sensations can be elicited through neurostimulation. However, due to the nature of electrical signals, and the fact that the electrical stimulation pulses are often larger in amplitude compared to the underlying EMG signal, the stimulation pulses can also be picked up by the nearby EMG electrodes. This creates unwanted artifacts in the activation patterns used to detect the user's intent and leads to reduced pattern recognition robustness [9].

The problem of stimulation artifacts is not only present in the area of prosthesis control, but also applies to any system involving closed-loop neuromodulation [10]. Literature on the topic of general artifact removal exists, but research involving prosthesis control applications is lacking. Moreover, the existing literature mostly focuses on removing electrocardiogram (ECG) artifacts from the EMG signals and do not consider the artifacts caused by neurostimulation for providing tactile feed-

back. Therefore, there is a need to develop and test methods to remove stimulation artifacts from implanted EMG electrodes.

1.1 Aim

On the basis on the lack of previous work in the field, the aim of this master's thesis project is to investigate, implement, and evaluate two algorithms for removing stimulation artifacts from EMG control signals on an embedded prosthesis controller in real time. Focus lies on EMG control signals stemming from the use of an osseointegrated prosthesis, with the goal to not updating the existing pattern recognition algorithm to also function correctly during stimulation.

1.2 Scope and Limitations

As the work focuses on development and implementation of artifact removal algorithms, there are some elements that will not be dealt with in this thesis. Firstly, no design of mechanical or electrical circuit components were made as this project focuses on utilizing an existing hardware platform. Furthermore, no development of pattern recognition and/or neurostimulation algorithms was performed.

1.3 Questions

Based on the thesis purpose, the following questions will be answered throughout the work:

- What effects do the stimulation artifacts have on the commonly used signal features for myoelectric pattern recognition?
- Can the algorithms sufficiently reduce the artifact effects?
- Are the investigated algorithms feasible to be used in real time on an embedded system?

By answering these questions, the goal is to evaluate the ability of the developed algorithms to improve prosthesis control for users of osseointegrated implants with nerve cuff stimulation.

1.4 Outline

The rest of the thesis is organized as follows: Chapter 2 provides more background and a review of previous work in the field of artifact removal. Next, Chapter 3 contains an overview of the experimental setup and the algorithms that were evaluated together with the evaluation scheme, and Chapter 4 contains the corresponding results. Finally, Chapter 5 and 6 provide a discussion of the method and the results, and concludes the thesis.

2

Background

This chapter is divided into two main parts. First, an introduction to the field of biosignals and prosthetic control is given to provide the reader with enough background to further understand the topic and chosen methodology. Then, an overview of previous work within artifact removal is presented together with some of the most common approaches to removing artifacts and their strengths and weaknesses.

2.1 Electromyography

Elecromyography is a technique for recording and processing muscle activation signals. The recorded signal, known as an electromyogram (EMG) signal, reflects the electrical activity of skeletal muscles and contains information about the intent of the underlying neural signals [11]. On a high level, the skeletal muscles are made up of groups of varying number of muscle fibers, so called *motor units*. Each motor unit is connected to a separate *motor neuron*, which is activated by *action potentials* transmitted from through the peripheral nervous system. Activation of a motor unit causes the connected muscle fibers to contract by firing action potentials along them, yielding a so called Motor Unit Action Potential (MUAP). Depending on where the EMG electrodes are placed, the EMG signal is a summation of all MUAPs caused by the nearby motor units [11].

There are two main ways of recording EMG signals: using very localized invasive needle electrodes, or in a non-invasive manner by placing surface electrodes on the skin, so called surface electromyogram (sEMG). Naturally, the surface electrodes provide more limited spatial resolution of the recorded signal, while higher MUAP frequencies are attenuated through the skin [11]. For people with amputations, further work has also been performed to isolate neural signals using Targeted Muscle Reinnervation (TMR), where nerves in the remaining limb are innervated into existing musculature and provide additional independent EMG signals [4].

2.2 Myoelectric prosthesis control

Myoelectric prosthesis control can be divided into three main areas: simple threshold-based methods, pattern recognition control, and regression control [12].

Threshold-based
The threshold-based approaches use EMG activity from a single muscle or from two

opposing muscles to trigger actions based on the the level of contraction. The methods can also be augmented to additionally allow proportional control of the speed or force of the movement by incorporating knowledge of the contraction strength. One common threshold-based approach is *direct control* where each electrode is directly linked to a movement such as opening/closing the prosthetic hand or rotating the wrist [12]. The level of contraction is often measured in terms of the Mean Absolute Value (MAV) of the signal [13], [14].

Naturally, the threshold-based approaches require many EMG signals as the number of degrees-of-freedom to control increases. Using methods such as TMR might therefore be beneficial to extend the number of accessible signals [4]. Furthermore, they suffer from *crosstalk* caused by muscles contracting together which requires fine-tuning of the thresholds for robust control. The control is also sequential by nature, meaning that only one movement can be performed at a time [12].

Pattern Recognition

The pattern recognition methods aim to overcome the requirement of more EMG channels by incorporating statistical and machine learning-like concepts to detect patterns in the EMG signals [12], [13]. Figure 2.1 shows a typical signal processing pipeline used for EMG pattern recognition.

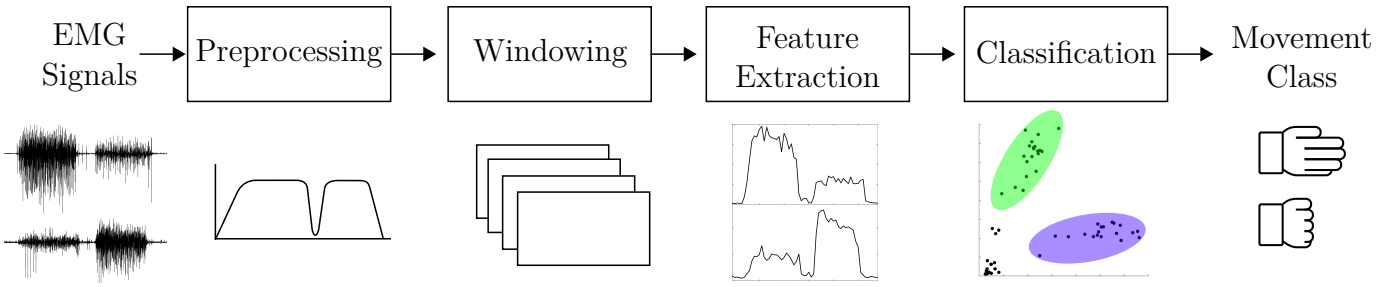

Figure 2.1: *A typical signal processing pipeline for myoelectric pattern recognition. Inspired by [13].*

The acquired EMG signals are first preprocessed to remove any unwanted interference such as power line noise. Then, the signals are divided into time windows from which signal features are extracted to be used by the classifier [13]. The time windows are usually on the order of $100 - 300$ ms long [12], [13] and can optionally overlap each other to provide a higher update rate.

A common set of features used for myoelectric control are the Mean Absolute Value (MAV), Zero Crossings (ZC), Slope Sign Changes (SSC), and Waveform Length (WL) features [14]. Together, these features capture measures of the waveform amplitude, frequency and duration characteristics without requiring complex calculations or frequency transformations. They are therefore well suited to be used on an embedded system with limited computing power where computational complexity is of great importance.

After calculating the features, they are passed on to classifiers such as Linear Discriminant Analysis (LDA) or Support Vector Machines (SVNs) [13]. The classifiers are trained in a supervised manner by recording signals with known movements

and using the algorithms to learn appropriate decision boundaries and/or class-conditional distributions. The classifiers are then used to predict the intended movement of the prosthesis user and control the device. Naturally, the pattern recognition performance relies on the distribution of the feature values for each movement/class to be sufficiently separable. If they are not, performance will quickly degrade.

Regression Control
Even though pattern recognition methods are able to use fewer EMG channels for decoding more degrees-of-freedom, they are still sequential by nature due to their discrete classifiers. Therefore, regression control methods have been developed to allow for simultaneous and proportional control. They provide continuous estimates of multiple control signals from the EMG signals and thus accommodate more flexible and intuitive control for the user [12].

2.3 Somatosensory feedback

In recent work, neurostimulation has been used to provide somatosensory (tactile) feedback in prosthesis devices [5]. By applying electrical currents to electrodes placed inside or wrapped around nerves in the residual limb, such as spiral cuff electrodes [15], sensations originating from the missing limb can be elicited [8].

Figure 2.2 shows an example of a typical asymmetric, biphasic, square pulse used for stimulation [15]. By changing parameters such as stimulation pulse frequency (F), pulse amplitude (I), and pulse width (PW), the perceived sensation of the stimulation can be changed. However, more research is required to provide natural sensations similar to those elicited in the intact limb [16].

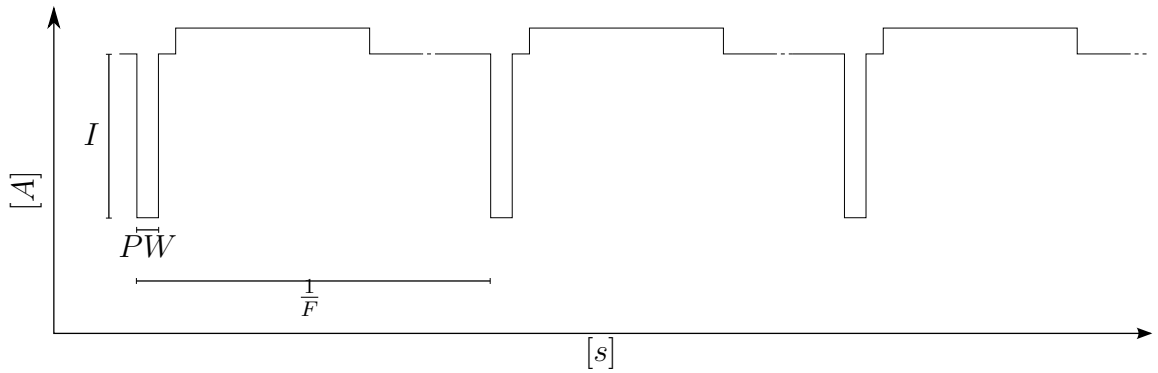

Figure 2.2: *A typical asymmetric, square, biphasic stimulation pulse used for somatosensory feedback. The stimulation pulse frequency (F), current (I) and pulse width (PW) can be varied to elicit different sensations. Inspired by [15].*

2.4 Stimulation artifacts

Even though the use of osseointegrated prostheses has provided improved resilience towards motion artifacts and other interference [8], the problem of stimulation artifacts still remains. When electrical currents are sent into the body to provide

sensory feedback, the stimulation potentials naturally spread throughout the surrounding tissues and interfere with the signals simultaneously measured on the EMG electrodes.

Generally, an artifact is comprised of two main components: a short larger *direct* artifact and a longer *residual* artifact [10]. The larger *direct* artifact is caused by the constant current stimulation pulses inducing charge in the stimulation electrode. The difference in charges causes a potential difference that affects the nearby EMG electrodes though the nonlinear dynamics of the human tissue, which in turn causes large voltage spikes to appear in the acquired signals. Ideally, the amount of charges delivered during the two opposite phases of the common biphasic stimulation pulse are equal and thus cancel each other out; ultimately leaving no residual charge left on the electrodes. However, a small mismatch in the constant-current drivers or variations in the pulses' lengths yield an imbalance in the delivered charge and cause the *residual* artifact to appear as a slow exponential tail when the residual charge bleeds out through the tissues.

Due to spectral overlap between the artifacts and the EMG signal, these artifacts can often not be removed using standard frequency filtering techniques, but instead require other methods to minimize the information loss [17].

2.5 Artifact removal

When working to mitigate the impact of stimulation artifacts on the recorded signals, there is generally a three step process to follow: (i) optimize the stimulation procedure to prevent artifacts in the first place, (ii) design the hardware front-ends to be more resilient towards artifacts, and (iii) remove the remaining artifact through software back-end processing [10]. Optimally, all three components should be designed considering the effects of the others to yield a complete system that is highly resilient to artifacts.

2.5.1 Artifact prevention

The first step is to prevent stimulation artifacts from appearing at all. There are multiple methods for solving this issue which are directly related to the stimulation hardware. To eliminate the difference in the positive and negative current sources, as is often caused by acceptable manufacturing inaccuracies [18], the same current source can be reused for both phases of the biphasic stimulation pulse using an H-bridge configuration [19]. Additionally, circuitry to either actively drive, or passively discharge [19] the stimulation electrode potential back to a common reference voltage can be used to shorten the residual artifact duration [10].

Attempts have also been made to isolate the stimulation and signal acquisition hardware to eliminate the common ground connection and thus allowing the acquisition circuitry to track and reject the stimulation artifacts as a common-mode signal [20]. Furthermore, the electrode placement can be of significant importance and used to reduce the artifact in the acquired signals [21].

2.5.2 Hardware front-end

After minimizing the artifact occurrence, the next step is to design a hardware front-end to be resilient towards the artifacts that remain.

One way to eliminate a large portion of the artifact is to use bipolar measurements [10], [21]. Instead of referencing each electrode to a common reference electrode, the signals from two nearby electrodes, preferably placed at each end of the target muscle, are subtracted to yield a differential signal. Since the electrodes are localized closer to each other than to the reference electrode, they have a larger probability of experiencing similar stimulation artifacts, which can then be eliminated as common-mode during differential amplification.

Zhou *et al.* [10] also shed light on two other important considerations, namely *saturation prevention* and *rapid recovery*. As the biosignal of interest often has a very small amplitude, the amplifiers are designed with a high gain. However, the high gain often leads to saturation of the amplifier when the stimulation artifacts with high signal amplitude are amplified. Even if no saturation occurs, the high-amplitude signal often reaches the non-linear region of the amplifier and as such makes the artifact harder to remove later in software due to the non-linear distortion of the signal. By increasing the dynamic range of the amplifier, the saturation can be avoided while leaving the full artifact in the linear amplifier region [10].

Even when no saturation occurs, many amplifiers use high-pass filters to block any DC offset. These filters have an inherent time constant which further contributes to a longer exponential *residual artifact* tail. Therefore, designing the front-end for *rapid recovery* from large saturating amplitudes is crucial [10].

Rapid recovery can be achieved with various techniques. The most common approaches include using special circuitry to actively reset the amplifier to a predefined baseline voltage after stimulation [18], and/or employing a resetting Analog-to-Digital Converter (ADC) and amplifier such that each sample is completely memoryless [19]. Analogous to the residual charge on the stimulation electrodes, any residual charge buildup on the recording electrodes can also be actively or passively reset to a common reference potential to shorten the residual artifact duration [10].

2.5.3 Software back-end

Finally, any stimulation artifact that is left in the signal after acquisition has to be handled in the software back-end. Herein lies the main focus of this thesis. Zhou *et al.* divides the methods for dealing with stimulation artifacts on the software side into three main categories: data reconstruction, artifact subtraction, and component decomposition [10].

Data reconstruction

In data reconstructing, the signal contaminated by the stimulation artifact is completely replaced by a reconstructed artifact-free version. This can be done in several ways, where the simplest one is to just replace the contaminated samples with zeros, so called *blanking* [9], [22]. Replacing the samples with the last known value using

sample-and-hold or the mean of the rest of the signal is also possible [23]. More advanced methods involve linear [24]–[26] and cubic-spline [27] interpolation between the signal value at the start and the end of the artifact period, or reconstruction based on estimated Gaussian distributions [25].

Due to the nature of the data reconstruction approach, that the sample values are replaced by new values, most information in the signal is lost during the reconstructed period. This is especially true for the blanking approach and limits the usage of data reconstruction techniques for practical applications. For example, if the artifact has a duration that is on the same time-scale as the biosignal of interest, too much information could be lost which renders the resulting signal useless. However, if the duration is much shorter, then data reconstruction techniques can be used for successful artifact removal [24].

Considering the information loss, Hartmann, Došen, Amsuess, *et al.* [9] investigated the implications for classification performance using the same feature set as presented in Section 2.2 above. They investigated three main means of dealing with the intervals of lost information: (i) to zero out the signal (blanking) and calculate the features as usual, (ii) to remove the contaminated samples and calculate the features on a shorter signal segment, and (iii) to remove the contaminated samples but wait longer to fill the entire original time window with samples before calculating the features. Based on experiments with sEMG, they concluded that approach (ii) and (iii) were preferred when the ratio of contaminated samples increased, and that (ii) was preferable for real-time usage as (iii) incurs unpredictable delays due to the additional time required to fill up the entire window [9].

Naturally, data reconstruction methods require the samples containing artifacts to be reliably detectable. Depending on the artifact waveform and its duration, this could be a more or less challenging task if no direct synchronization signal from the stimulation device is available. A common approach is to rely on the large artifact spikes by using a combination of signal peek detection and thresholding [22], [25], [28].

Artifact subtraction

Using artifact subtraction techniques, artifacts are removed by subtracting an estimate of the artifact from the signal. Naturally, this assumes that the stimulation artifact is linearly additive with respect to the underlying biosignal and thus that the artifact stays within the linear range of the amplifier [29].

The technique can be further divided into two subcategories: template subtraction and adaptive filtering. In template subtraction, a template of the artifact is, for example, estimated from previous samples using moving average with exponential forgetting [30], or by using Finite Impulse Response (FIR) or Infinite Impulse Response (IIR) filters [31]. Other approaches involve estimating the exponential tail as an autoregressive (AR) process [28] or by fitting a polynomial around each sample, which also requires knowledge of future samples [32]. Methods have also been proposed that use neural networks or several linear estimators to predict the artifact tail based on the area of the first large signal spike [33].

Similar to data reconstruction methods, most of the template subtraction techniques rely on detection of the stimulation onset. Therefore, unless a reliable synchronization signal is available, the onset has to be detected by analyzing the signal samples directly.

Depending on the template estimation method applied, the template subtraction methods might have difficulties adapting to fast-changing stimulation artifact waveforms. This is especially true for those estimators that rely on averaging previous artifacts [29], while the methods relying on local curve fitting or AR processes are more likely to adapt to changing artifact waveforms due to them being less reliant on previous artifacts.

Adaptive filtering techniques, on the other hand, do not estimate the artifact waveform directly from the acquired samples. Instead, they assume that the artifact and biosignal are uncorrelated and rely on a reference signal highly correlated with the artifact. A linear mapping between the artifact and the reference is then learned with the objective to minimize the Mean Squared Error (MSE) between the prediction and the true signal [17], [34]. The technique was first introduced for adaptive noise canceling by Widrow *et al.* in the form of the Least Mean Squares (LMS) filter [35] and has since also been used for removing various artifacts in biosignals such as ECG [36]. The standard LMS algorithm has been further developed and derivatives such as Normalized Least Mean Squares (NLMS) and methods based on Recursive Least Squares (RLS) have also been used to remove artifacts with promising results [37], [38].

For removal of stimulation artifacts, the filter reference signal is usually selected as either a synchronization pulse coming from the stimulation device [39], or a signal recorded by a nearby electrode not containing the biosignal of interest [37]. In some settings, a previous artifact can also be replayed together with the current acquired signal to act as a reference [40]. By simplifying the LMS scheme, adaptive filtering can additionally be implemented in hardware, for example as the Sign-Sign LMS algorithm [39].

One major drawback of the standard adaptive filtering scheme is the assumption of a linear relationship between the reference and the artifact. In order to combat this, Grieve *et al.* exchanged the linear LMS adaptive filter with a feed forward multilayer perceptron (MLP) neural network updated using back-propagation [40]. Compared to an adaptive RLS filter, they saw improved results using their MLP based filter which was better suited for modelling nonlinear relationships.

On the other hand, the adaptive filtering and to some extent also the template subtraction scheme, have the advantage that they remove the artifacts even though the frequency spectra of the artifact and the biosignal overlap [38] since no explicit frequency-based filtering is performed.

Component decomposition

Techniques relying on component decomposition usually follow a general process of decompose-remove-recreate. In the decompose step, the recorded signal(s) are decomposed using some sort of Blind Source Separation (BSS) method such as

Independent Component Analysis (ICA) , Canonical Correlation Analysis (CCA), Wavelet Transform (WT), or Empirical Mode Decomposition (EMD) to separate the signals into several components. Next, the components containing artifacts are detected and either removed or modified to suppress the artifacts. In the final step, the remaining components are used to reconstruct the artifact-free signal(s) again [10], [17].

These techniques have been successfully applied for removing general artifacts in biosignals [41], [42] and also for stimulation artifact removal in EMG [43] and electroencephalogram (EEG) [44] signals. While they generally provide great accuracy in the resulting artifact-free signal, they are also often significantly more computationally expensive in comparison to the other techniques making them less feasible for real-time usage on low-end hardware [10].

Additional methods

In addition to the above mentioned categories, there are also a few more techniques for removing artifacts. One such approach is to use Bayes filters [17]. In short, the Bayes filter makes use of a predictor-corrector structure where the predictor uses the current state to predict a future state based on a probabilistic model. The corrector then uses another probabilistic model to incorporate the measurements into the predicted state. An example of a Bayes filter is the Kalman Filter, in which states are represented by Gaussian distributions and the models are simple linear transformations. Due to the usage of Gaussian distributions, the Kalman filter is only able to handle unimodal state distributions. Another implementation of a Bayes filter, the so called particle filter, is however able to cope with multi-modal state distributions and also has no restriction on the use of linear models [17].

3

Method

This chapter contains the methods used throughout the thesis work. It gives an overview of the used hardware platform, the performed experiments, the algorithms that were selected, and how they were evaluated in the offline and preliminary online setting.

3.1 Hardware

The hardware used throughout the experiment and signal acquisition was based on previous work by Mastinu et al. [45]. It was comprised of the same TM4C123GH6PM 32-bit ARM Cortex-M4F main Microcontroller Unit (MCU) running at 80 Mhz (Texas Instruments, USA) but accompanied by a secondary MSP430G2755 16-bit mixed signal MCU at 16 Mhz (Texas Instruments, USA). The signal acquisition and stimulation was performed by a RHS2116 digital electrophysiology stimulator and amplifier chip (Intan Technologies, USA).

In Figure 3.1, an overview of the system and the responsibilities of each of the three chips is given. At the lowest level, the RHS2116 acts as a bridge between the human body and the rest of the controller and is connected directly to the electrodes used for stimulation and EMG signal acquisition. It generates the constant-current stimulation pulses and amplifies and digitizes the low-amplitude EMG signals by using a configurable DC or AC-coupled amplifier and a single ADC capable of sampling 16 amplifier channels at 40 kHz each [46]. The amplifiers also feature configurable low- and high-pass filters for initial signal filtering. The interested reader is referred to the RHS2116 datasheet [46] for more information.

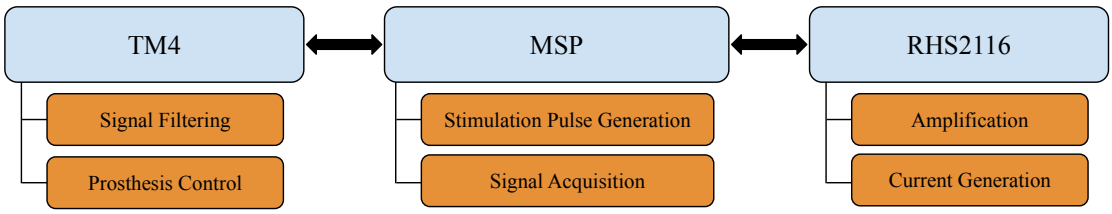

Figure 3.1: *An overview of the components of the hardware platform. The TM4 performs high-level signal processing and controls the prosthesis while the RHS2116 interfaces directly with the electrodes and amplifies the EMG signals. The MSP is used to sample multiple channels and generate the timing for the stimulation pulses.*

As the RHS2116 requires constant updates to generate the correct timing for the stimulation pulses and sampling of the channels of interest, the secondary MSP microcontroller is used to act as a higher-level interface to be used by the TM4 main processor. It receives requests for stimulation and channel acquisition from the TM4 and communicates with the RHS2166 chip to satisfy them.

Due to the tight timing requirements of the stimulation pulses, the MSP microcontroller is completely occupied with generating the stimulation signal during a stimulation phase and therefore does not allow for any signal acquisition during this time period. This poses a problem as the EMG signal is completely lost during the stimulation pulse generation and thus incur a form of forced *blanking*[9], [22]. However, this provides a useful indicator signal that can be used to synchronize the artifact removal algorithms with the stimulation pulse onset.

Finally, the TM4, with its built-in floating point unit, performs high-level signal filtering and buffering, feature extraction, motion classification, and control of the prosthesis. This is also when the stimulation artifact removal algorithms are applied before the feature extraction step. The TM4 also handles external communication over Bluetooth and allows for tethering to a computer for signal streaming and remote control.

As the RHS2116 chip allows for stimulation and signal acquisition on the same channel, a reference signal can be recorded by acquiring samples from the stimulation channel after the stimulation period has ended. Figure 3.2 shows an example of an EMG signal (bottom), the corresponding reference (top), and stimulation active synchronization signal (middle). These three signals are available for use by the stimulation artifact removal algorithms.

The RHS2116 also contains a few hardware features for reducing the effect the stimulation artifacts have on the acquired samples. The *low-frequency cutoff shifting* feature allows the low-frequency cutoff of the AC-amplifiers to momentarily change to an alternative (higher) frequency. This improves the transient response after a possible amplifier saturation due to a large stimulation artifact. To further improve the recovery from saturation, the *amplifier fast settle* functionality allows the amplifiers to be reset to a baseline voltage. Finally, the *charge recovery switch* can be activated to briefly connect the electrode to a common ground to bleed out any residual charge [46].

Table 3.1 contains the parameters that were used throughout all the experiments. The *low-frequency cutoff shifting* and *charge recovery switch* were also activated for all channels during an extra 1 ms after each stimulation pulse to improve artifact recovery.

Table 3.1: *The hardware parameters that were used throughout all experiments.*

Sampling frequency	1000 Hz
Amplifier low-frequency cutoff	20 Hz
Alternate low-frequency cutoff	1000 Hz
Amplifier high-frequency cutoff	1000 Hz

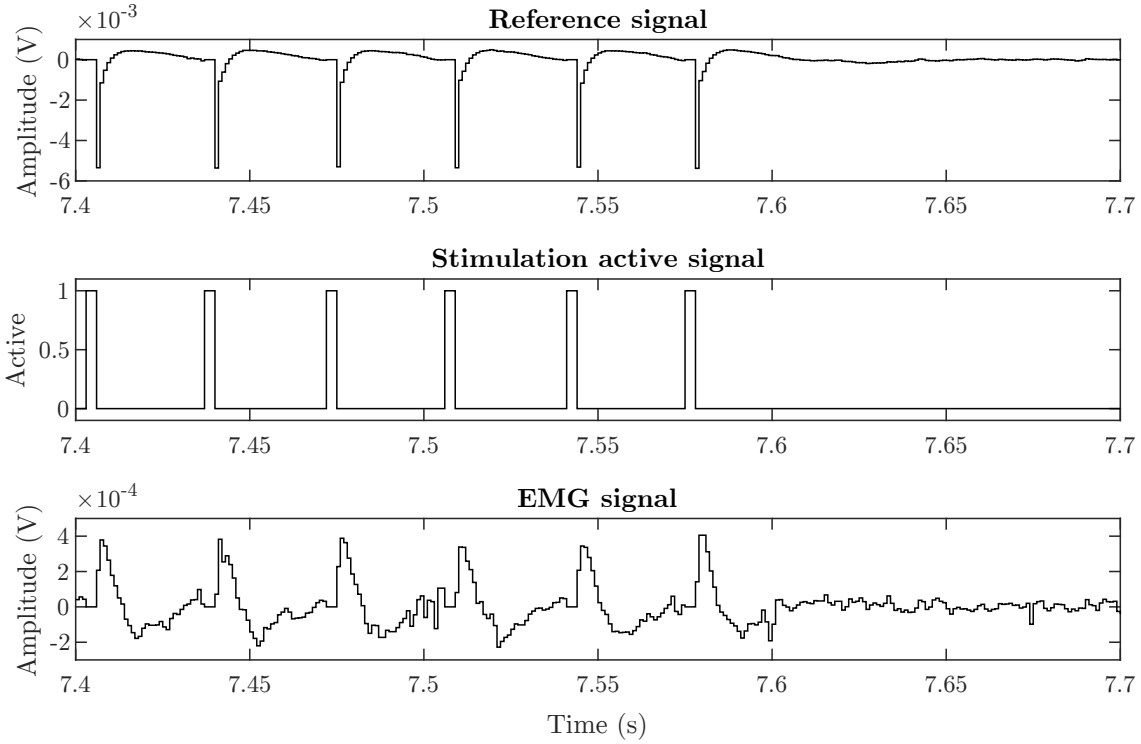

Figure 3.2: *An example of the signals available to the artifact removal algorithms. Top: reference from the stimulation channel, middle: stimulation active synchronization signal, bottom: EMG signal to filter. Note the regular shape of the artifact tail in the EMG signal.*

3.2 Experimental setup

Data was collected in two main experiments: the initial data collection experiment and the preliminary online evaluation experiment. This section describes the used experimental setup and the data collected for the initial data collection, while Section 3.6 elaborates on the preliminary online experimental setup and evaluation procedure.

The experiment consisted of one male participant with a transhumeral (above-elbow) amputation and an osseointegrated e-OPRA implant [6] connected to a daily used prosthetic arm as previously reported by Ortiz-Catalan, Mastinu, Sassu, *et al.* [8]. The participant had used his myoelectric prosthetic arm for more than two years. Signal recordings were obtained from five electrode channels normally used for controlling the prosthesis using direct control, including the stimulation channel itself as a reference and the channels associated with the hand *open*, *close*, *pronate* and *supinate* prosthesis movements. From now on, the channels will be referred to based on their associated prosthesis movement.

The EMG signals were recorded by the hardware platform and sampled at 1000 Hz. The signal was then filtered through a 50 Hz notch filter to reduce electrical interference and a second order high-pass filter at 20Hz to remove any remaining low-frequency components. Stimulation was applied through an implanted extraneural

spiral-cuff electrode located around the median nerve.

For each recording, the participant was asked to perform three different scenarios: (i) no movement, (ii) repeated hand close and open movements or (iii) repeated hand pronate and supinate movements. The signals in scenario (i) were recorded for 10 seconds, while scenarios (ii) and (iii) were recorded for 15 seconds each. During the first half of the recording, stimulation was applied in the form of multiple successive pulses delivered at the stimulation frequency. Suitable stimulation parameters were chosen based on initial tests of the participant's detection threshold, see Table 3.2. Each scenario was repeated once for each of the four parameter sets. In total, 12 recordings were obtained.

Table 3.2: *Stimulation parameter sets used for the data collection experiment. Specific values were chosen based on tests of the participant's detection threshold.*

Amplitude [μA]	Pulse width [μs]	Frequency [Hz]
300	150	30
450	150	30
300	150	50
450	150	50

3.3 Algorithms

Based on the hardware platform and its limitations and previous work in the field (see Section 2.5.1), two algorithms for stimulation artifact removal were selected for implementation and evaluation. In an initial screening of algorithm selection, the algorithms based on decomposition were considered to be too computationally expensive to justify the performance. Previous work involving general artifact removal using decomposition methods have often involved offline computation [42], [43] and mentioned the need for considerably more powerful hardware if real-time operation is desired [41], [44]. Sweeney *et al.* [17] also mentions that most decomposition-based algorithms are not suitable for online usage, and according to Zhou *et al.* (2018) these methods have not yet been implemented for online real-time use [10].

On the other hand, previous work by Maier *et al.* [47] and Naber *et al.* [48] has shown that filtering and feature extraction based on Discrete Wavelet Transform (DWT) was feasible on a similar real-time embedded system as used in this thesis. However, given the availability of reference and synchronization signals on the hardware platform and that computational complexity is of large importance, other simpler-to-implement algorithms were chosen.

3.3.1 Algorithm A: Template Subtraction

As the first algorithm, a simple Template Subtraction (TS) algorithm based on a first order infinite impulse response (IIR) filter, similar to the methods presented by Keller *et al.* [30] and Azin *et al.* [31], was implemented. The algorithm was chosen due to its simplicity and recursive formulation which yields a very computationally

efficient implementation for usage in real-time on an embedded device with limited resources.

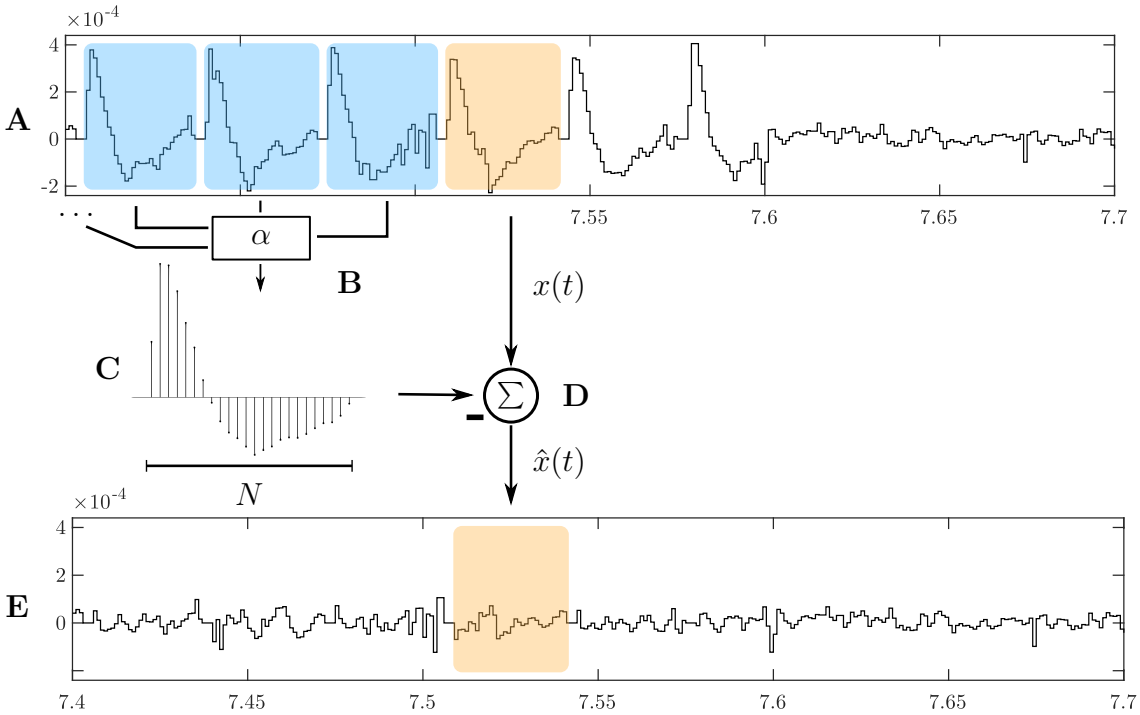

Figure 3.3: *Illustration of the TS algorithm. (**A**) The original signal $x(t)$. Previous artifacts (blue) are averaged (**B**) using exponential filters to form the template (**C**). The template is subtracted (**D**) from the original signal to yield the estimated artifact-free signal $\hat{x}(t)$ (**E**).*

Figure 3.3 illustrates the working principle of the algorithm. In short, the algorithm constructs a representative template of the stimulation artifact by averaging the N first samples of artifacts from previous stimulation pulses using multiple moving average exponential filters with filtering coefficient α. The template is then subtracted from the original signal $x(t)$ to yield an estimated artifact-free signal $\hat{x}(t)$.

Let N be the length of the template to average, α be the filtering constant, the *learning rate*, and let $W_k(i)$ represent the learned artifact at sample $i = 1, \ldots, N$ after the end of stimulation pulse k. Assuming that t_k is the sample index at which stimulation pulse k ends, i.e., when the stimulation synchronization signal goes from high to low, the recursive update is defined by Eq. (3.1):

$$W_k(i) = \begin{cases} (1-\alpha) \cdot W_{k-1}(i) + \alpha \cdot x(t_k + i - 1), & i = 1, \ldots, N, \\ 0 & i > N, \end{cases} \tag{3.1}$$

and the estimated artifact-free signal is then given by Eq. (3.2):

$$\hat{x}(t_k) = x(t_k) - W_k(i), \quad i = 1, \ldots, N. \tag{3.2}$$

For ease of implementation, the above recursive formulation can be written in the form of a sample-by-sample update procedure as in Algorithm 3.1.

Note that after the template ends, i.e., when the template has been subtracted and no more stimulation pulses are being generated, the algorithm uses the unfiltered signal as its estimate of the artifact-free one. This is valid behavior under the assumption that the sampled signal does not contain any stimulation artifacts after N samples has passed.

Algorithm 3.1 Template Subtraction

```
i ← N + 1
for each sample t do
    if stimulation is active at t then
        i ← 0
    end if
    if 0 < i ≤ N then
        W_i ← (1 − α) · W_i + α · x(i)
        x̂(t) ← x(t) − W_i
    else
        x̂(t) ← x(t)
    end if
    i ← i + 1
end for
```

3.3.2 Algorithm B: Adaptive Filter

The second algorithm chosen for implementation was an adaptive filter based on an extension of the common LMS algorithm. The LMS algorithm and its variants have been used successfully in previous work on artifact removal [37], [39] and also has the possibility of improved adaptability to varying stimulation conditions due to the usage of a reference channel correlated with the artifact source.

In this context, the LMS adaptive filter is used to predict the artifact based on a linear mapping / convolution from the reference channel as can be seen in Figure 3.4. Similar to the previous algorithm, the predicted artifact is then subtracted from the signal $x(t)$ to yield the estimated artifact-free signal $\hat{x}(t)$.

Theoretical Overview
In general, the LMS algorithm is a stochastic-gradient algorithm for iteratively solving the linear least-mean-squares estimation of a zero-mean scalar random variable d given another zero-mean random vector $\boldsymbol{u}$ [34]. Assuming that both d and $\boldsymbol{u}$ are real-valued, the estimation problem can be expressed in terms of the optimization problem (3.3)

$$\min_{\boldsymbol{w}} \mathbb{E}[d - \boldsymbol{w}^T \boldsymbol{y}], \tag{3.3}$$

where $\boldsymbol{w}$ is a $N \times 1$ weight vector. The closed-form solution for the optimal weight vector is given by Eq. 3.4

$$\boldsymbol{w}^o = R_u^{-1} R_{du}, \tag{3.4}$$

where $R_u = \mathbb{E}[\boldsymbol{u}\boldsymbol{u}^T]$ is the auto-correlation matrix of $\boldsymbol{u}$ and $R_{du} = \mathbb{E}[d\boldsymbol{u}]$ is the cross-correlation vector between d and $\boldsymbol{u}$ [34].

In most practical applications, however, the exact statistical properties of d and $\boldsymbol{u}$ are not known and calculating and inverting the auto-correlation matrix R_u is not feasible. Instead, assuming that multiple observations of d and $\boldsymbol{u}$ are available, denoted $\{d(0), d(1), \dots\}$ and $\{u(0), u(1), \dots\}$, respectively, the optimal weight vector

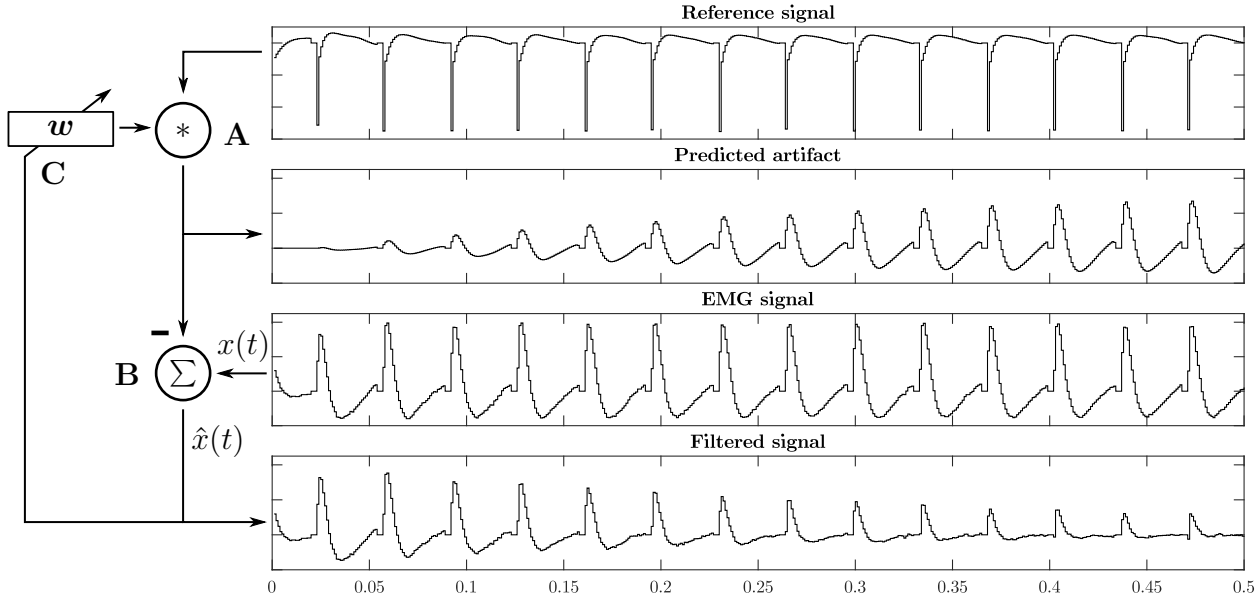

Figure 3.4: *Illustration of the adaptive filter algorithm for removing stimulation artifacts. The reference signal is convoluted with the filter weights* $\boldsymbol{w}$ *(**A**) to predict the artifact waveform. The predicted artifact is subtracted from the original signal* $x(t)$ *(**B**) to yield an estimated artifact-free signal* $\hat{x}(t)$ *which is then also used to update the filter weights after each sample (**C**).*

can be approximated iteratively via the recursive LMS update rule (3.6):

$$e(i) = d(i) - \boldsymbol{w}^T u(i) \tag{3.5a}$$

$$\boldsymbol{w}_i = \boldsymbol{w}_{i-1} + \mu u(i) e(i), \tag{3.5b}$$

where $e(i)$ denotes the estimation error at iteration $i \geq 0$ and $\mu > 0$ is a step-size [34].

The observant reader might note that the actual change made to the filter weights $\boldsymbol{w}_i$ in each iteration is highly dependent on the norm of the vector $u(i)$. Thus, an observation with a large norm will normally lead to a larger change to $\boldsymbol{w}_{i-1}$ than an observation with a smaller norm. This is especially important when filtering signals where high activity intervals are followed by intervals of lower activity such as speech and EMG signals. To mitigate this dependency, normalization and regularization can be applied to yield the ϵ-Normalized Least Mean Squares (ϵ-NLMS) update rule (3.6):

$$e(i) = d(i) - \boldsymbol{w}^T u(i) \tag{3.6a}$$

$$\boldsymbol{w}_i = \boldsymbol{w}_{i-1} + \frac{\alpha}{\epsilon + ||u(i)||^2} u(i) e(i), \tag{3.6b}$$

where α is a positive step-size parameter and ϵ a small positive parameter used to avoid division by zero. The ϵ-NLMS method can also be seen as a variant of the Newton method for iterative optimization, and thus inherits its faster convergence behavior compared to the simpler LMS algorithm. For further theoretical derivations, the interested reader is referred to the book by Sayed [34].

Application to artifact removal
When applying the adaptive LMS and ϵ-NLMS filters with the goal to remove stimulation artifacts, the iteration index i is replaced with the time sample index t. As the desired signal $d(i)$, the acquired artifact-contaminated EMG signal $x(t)$ is used and as observation of the predictor $\boldsymbol{u}$, the last N samples from the reference channel is used. In this configuration, the adaptive filter learns to predict the artifact from the reference signal and produces the estimated artifact-free signal $\hat{x}(t)$ as the estimation error $e(i)$ as seen in Figure 3.4.

Naturally, as the adaptive filter aims to minimize the squared estimation error $e(i)$, by updating the filter when there are no stimulation artifacts, it will learn to predict the *actual* EMG signal possibly picked up by the stimulation electrode as crosstalk from another muscle. To remedy this, the filtering process is only performed for the first $2N$ samples after each stimulation pulse while the subsequent acquired samples are left untouched. This behavior is similar to the one employed by algorithm A where the signal is untouched after subtracting the template.

3.3.3 Dealing with blanked samples

Due to the involuntarily blanking of samples during stimulation pulse generation, some of the information related to myoelectric activity is lost. The loss of information also effects the feature values and ultimately degrades pattern recognition performance. As previously investigated by Hartmann *et al.* [9], the situation can be improved by completely excluding the blanked samples from the acquired time window signals before calculating the feature values. Therefore, the same approach was used when calculating feature values in the evaluation of the algorithms and can be seen as a general addition to both algorithms.

3.4 Implementation

The two algorithms were first implemented in MATLAB to be used with the recorded signals for the offline evaluation. To improve computational speed and ease the implementation on the hardware platform, the algorithms were also implemented as C MEX functions using the MATLAB External Language Interface[1]. For the online evaluation step, the algorithms were implemented on the hardware platform in the C programming language.

3.5 Evaluation

Using the collected data, the chosen algorithms were evaluated offline in MATLAB and online on the embedded device. This section explains the used evaluation metrics and how the hyperparameters were optimized for optimal artifact removal performance.

[1] `https://mathworks.com/help/matlab/external-language-interfaces.html`

3.5.1 Hyperparameter optimization

Each of the two algorithms presented above contain two important hyperparameters; the integer filter/template length N and the real-valued learning rate α. Manually finding the parameters that optimally restores the original signal is a tedious task. Therefore, a hyperparameter optimization scheme was developed, where each channel was optimized individually due to the large variance in signal amplitude, EMG activity, and stimulation artifact influence.

To be able to measure and quantify to what extent the algorithms were able to remove the stimulation artifacts, two components were needed: (i) knowledge of the true underlying artifact-free signal and (ii) a measure of similarity between the estimated and the original signals.

A common practice for solving the first problem is to construct semi-synthetic signals by superimposing stimulation artifacts onto artifact-free EMG signals [27], [42], [43], as illustrated in Figure 3.5. Based on the recorded signals from the experiment, signal segments containing only stimulation artifacts, open and close movements, and pronation and supination movements were extracted for each of the four stimulation parameter sets in Table 3.2. The four artifact-only signals were then superimposed onto each of the eight artifact-free signals, yielding a total of 32 semi-synthetic signals for each channel. Additionally, the signals were blanked with zeros during the stimulation pulse generation to imitate the situation on the hardware platform during stimulation.

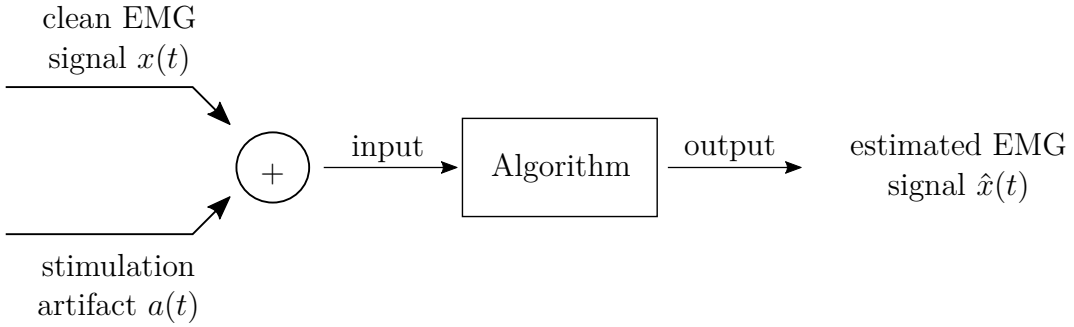

Figure 3.5: *Semi-synthetic signals are constructed by adding pure stimulation artifacts $a(t)$ to clean EMG signals $x(t)$ and processed by the algorithm to yield an estimated artifact-free signal $\hat{x}(t)$.*

As a measure of algorithm performance, the Root Mean Squared Error (RMSE) metric between the artifact-free signal $x(t)$ and the filtered signal $\hat{x}(t)$ was selected. This metric has been used successfully in previous research on artifact removal for evaluating algorithm performance [28], [43], and is defined in Equation (3.7).

$$RMSE = \sqrt{\frac{1}{L}\sum_{i=1}^{L}\left(x(i) - \hat{x}(i)\right)^2} \tag{3.7}$$

The final optimization objective was given by the median of the 32 RMSE values. The median was chosen to eliminate the effect of large outliers caused by possibly

difficult signal and artifact combinations. From a control and usability perspective, it is more valuable that the algorithm works the best in *most* cases and fails in a few as compared to having slightly bad performance over *all* situations.

The final optimization problem was a Mixed-Integer Nonlinear Programming (MINLP) problem as it included both integer and continuous variables, and therefore required special care. In this case, however, as there was only one integer variable that additionally had a limited range, it was enough to solve the problem using a brute-force method. By iterating through the possible values of the length N and applying the MATLAB optimization function `fmincon` to optimize for α, the global optimum could be found.

In our case, the range of the integer length N could be inferred from the stimulation parameters and sampling rate used during recording. At a sampling frequency of 1000 Hz and minimum stimulation frequency of 30 Hz, the maximum number of samples between each stimulation pulse was $1000/30 \approx 33$, of which a few were always blanked due to the hardware limitations. Therefore, the optimization was performed considering lengths in the range $N \in [1, 34]$.

3.5.2 Sensitivity analysis

One drawback of optimizing the algorithm parameters for a minimal reconstruction error is that the process requires previously recorded signals to be available. However, as the goal was to use the proposed algorithms in a real system, knowing how changes in the parameter values affect the overall system performance and ability to remove artifacts was important for easier manual configuration. Therefore, the sensitivity to variation in the hyperparameters N and α was investigated.

Using the same set of semi-synthetic signals as for the optimization procedure, the algorithms' hyperparameters were varied before applying them to the signals. However, using the RMSE between the true EMG signal $x(t)$ and the estimated artifact-free signal $\hat{x}(t)$ as a performance metric can be problematic for comparing performance between channels due to the large variation in signal amplitude. The RMSE is completely usable when optimizing algorithm performance, but as soon as comparing signals of different fundamental amplitudes, another metric is required. Additionally, the RMSE is difficult to interpret and relate in terms of absolute performance.

Therefore, a more general metric based on Signal-to-Noise Ratio (SNR), as employed in [37], was used for evaluating the algorithms' performance related to changes in the hyperparameters. The metric, hereby denoted as ΔSNR or SNR *improvement*, measures the change in SNR in decibels when applying the algorithm. It is not dependent on the absolute amplitude of the signals, but rather on the relative energy content of the true signal $x(t)$, artifact $a(t)$, and estimated artifact-free signal $\hat{x}(t)$,

as in Equation (3.8):

$$\begin{aligned}\Delta SNR &= SNR_{out} - SNR_{in} = \\ &= 10\log_{10}\frac{\frac{1}{L}\sum_{i=1}^{L}x^2(i)}{\frac{1}{L}\sum_{i=1}^{L}[\hat{x}(i)-x(i)]^2} - 10\log_{10}\frac{\frac{1}{L}\sum_{i=1}^{L}x^2(i)}{\frac{1}{L}\sum_{i=1}^{L}a^2(i)},\end{aligned} \tag{3.8}$$

where L is the length of the signals. To remove dependence on the number of blanked samples, the blanked samples were simply discarded in the same way as during feature value calculation as described in Section 3.3.3.

3.5.3 Effect on control features

To answer the question of how the stimulation artifacts affect the common features used for myoelectric pattern recognition, a similar scheme as described in section 2.2 was employed. First, all the recorded EMG signals were split into control windows of 100 samples each (corresponding to an update rate of 10 Hz when sampled at 1000 Hz) and labeled to indicate whether they contained stimulation artifacts and/or EMG activity for each channel. Next, the algorithms were applied to the signals and the feature values for each control window was calculated. Similarly, the features were also calculated for the unfiltered signals in order to evaluate the effect of the algorithms.

Violin plots were generated for visualizing the distribution of each feature during and in-between EMG activity for the cases without stimulation (*No S*), with stimulation only (*S*), and with stimulation applying each of the two algorithms (*S+A* and *S+B*, respectively). Violin plots have several advantages over classical box plots. For example, as they include a density estimation, they are able to better visualize clustered and multi-modal data, something that traditional box plots can struggle with [49].

The violin plots were generated using the MATLAB implementation by Bechtold [50]. The density was estimated using a Gaussian kernel with constant bandwidth within each channel, allowing for a qualitative visual inspection of the change in distribution and an indication of whether or not the algorithms were able to recover the feature value distributions during stimulation to be similar to the case when no stimulation was applied. Note that the scale of the axes was not important since the goal was to compare the distributions visually, but they have been left in the figures for completeness only.

3.5.4 Statistical analysis

To support the visual interpretation of the effect on the control features, statistical analysis using the non-parametric Wilcoxon-Mann-Whitney U-test was performed [51], [52]. The test was used to investigate if any statistical difference in distribution was found between the *No S* baseline case (without stimulation) and the three cases with stimulation applied; *S*, *S+A* and *S+B*, respectively, both during and in-between EMG activity. Ideally, the test should fail to conclude a difference in distribution when any of the two algorithms were applied (*No S* vs. *S+A* and *S+B*), while

potentially finding a significant difference in the case when they were not (*No S* vs. *S*).

Due to the large number of tests performed, Bonferroni correction was applied to the resulting p-values [53]. As the set of data containing EMG activity and the one without any activity can be seen as independent data sets, the correction was applied for each case separately by multiplying the p-values by the number of tests, in this case 48 (4 features $\times$ 4 channels $\times$ 3 tests each).

3.6 Online evaluation

Even though the online evaluation was still in progress at the time of writing this thesis, some preliminary tests had already been performed using a similar experiment as during the initial data collection. During this experiment, however, all algorithm calculations were performed on the embedded prosthesis controller and the signals streamed to a computer in real-time. To make the scenario as authentic as possible, the device was also responsible for generating stimulation signals in response to manually activating the sensor in the attached prosthetic hand. See Figure 3.6 for an illustration. Signals from the same participant (see Section 3.2) were recorded while performing the same four prosthesis movements and briefly activating the stimulation to overlap the EMG activity in the signal. The experiment was performed 13 weeks after the initial online experiment.

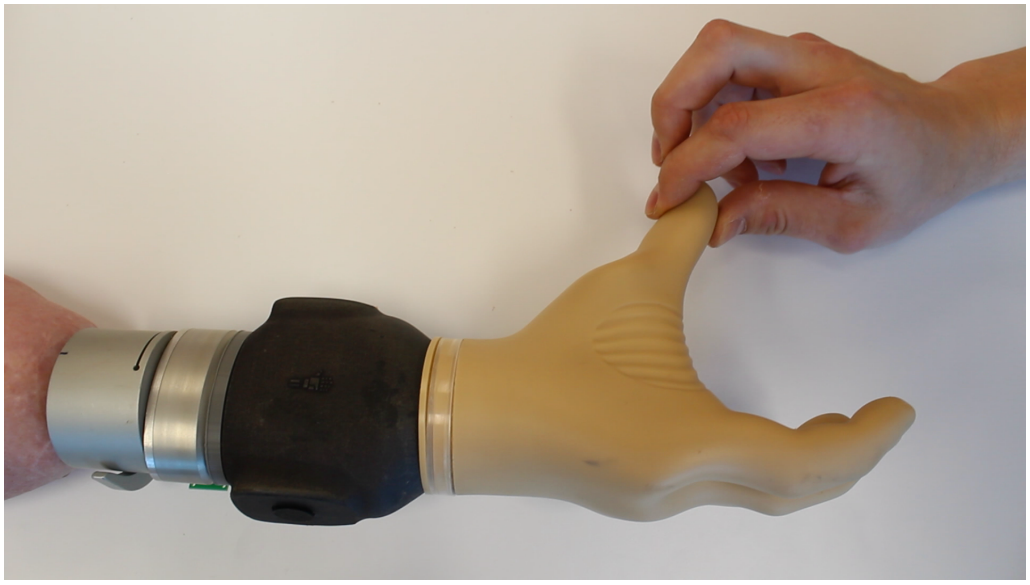

Figure 3.6: *The experimental setup during the preliminary online evaluation. Authentic stimulation feedback was generated by the prosthesis controller in response to manual activation of a sensor located in the thumb of the prosthesis, while raw and processed EMG signals were streamed to a computer in real time.*

The recorded data containing both the raw acquired signals and the signals processed by each of the two algorithms were then labeled based on EMG activity and

stimulation presence on each channel and processed similarly to the offline evaluation. For the purpose of demonstrating the real-time capability of the algorithms in this thesis, only the MAV features were calculated and visualized.

4

Results

This chapter presents the results and findings from the offline algorithm evaluation including parameter optimization, parameter sensitivity analysis, and the effect on the set of common features used for pattern recognition. It also presents the results from the preliminary online evaluation.

4.1 Hyperparameter optimization

Table 4.1 presents the optimal algorithm parameters found by optimizing the median RMSE between the true EMG signal and the estimated artifact-free signal on the set of generated semi-synthetic signals. In general, both algorithms performed better with longer template and filter lengths N, and low learning rates α. For the hand close channel, however, the optimal filter length for algorithm B was considerably lower than that of the other channels. Overall, Algorithm B seems to perform better than algorithm A, as it consistently yielded a slightly lower median RMSE on all channels.

Table 4.1: *Optimal algorithm hyperparameters found by minimizing the median RMSE reconstruction error between the true EMG signal and the estimated artifact-free signal on the set of semi-synthetic signals.*

Channel	Algorithm A (TS)			Algorithm B (ϵ-NLMS)		
	N	α	Median RMSE	N	α	Median RMSE
Open	24	0.0718	$3.409 \cdot 10^{-5}$	31	0.0529	$3.016 \cdot 10^{-5}$
Close	18	0.0467	$4.307 \cdot 10^{-5}$	9	0.0126	$4.109 \cdot 10^{-5}$
Pronate	18	0.0984	$2.101 \cdot 10^{-5}$	31	0.0629	$2.082 \cdot 10^{-5}$
Supinate	23	0.0200	$9.590 \cdot 10^{-6}$	34	0.0096	$8.957 \cdot 10^{-6}$

4.2 Sensitivity analysis

The results of the sensitivity analysis for changes in the algorithm hyperparameters are shown in Figure 4.1 and 4.3 where the learning rate α and template/filter length N are varied, respectively, while keeping the other parameter at the optimum value from Table 4.1.

Learning rate

As can be seen in Figure 4.1, larger α generally seems to lead to more variability

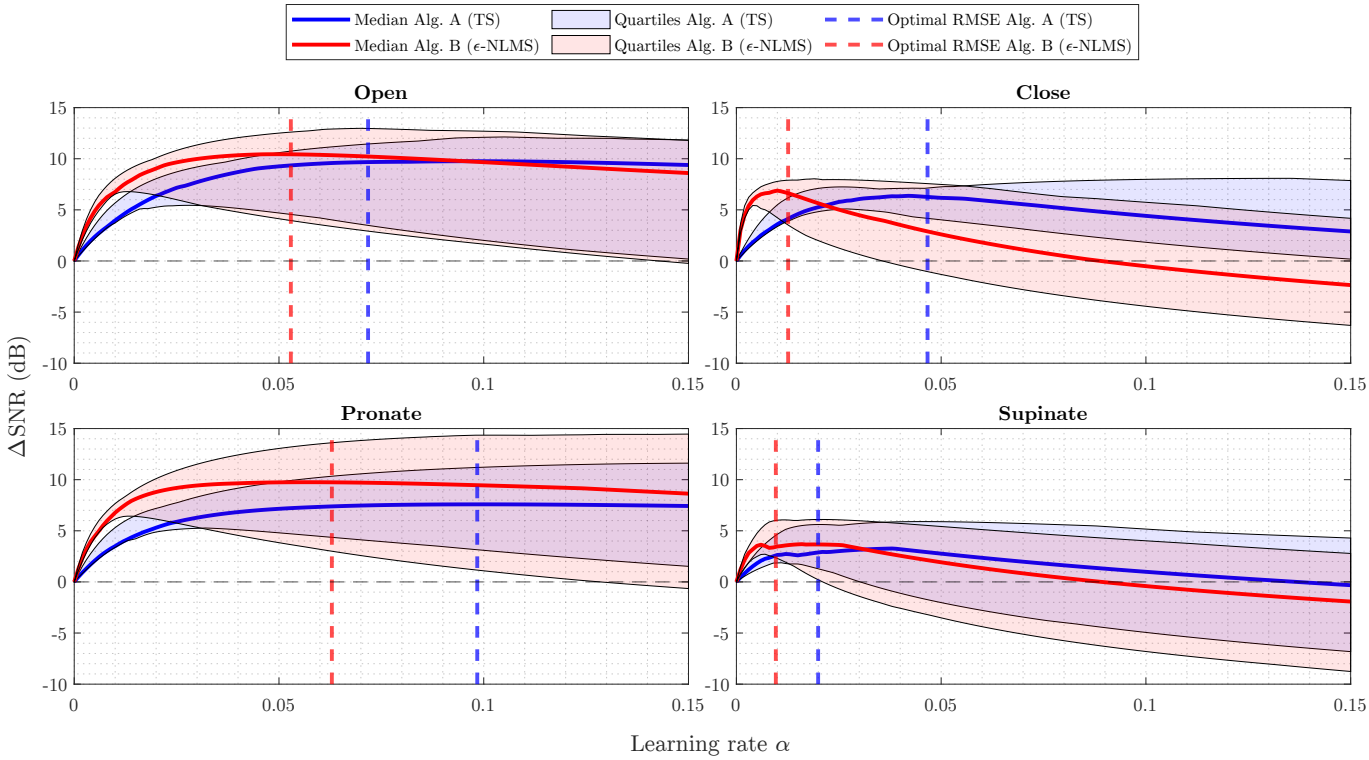

Figure 4.1: *Change in SNR per channel while varying the learning rate α for algorithm A (blue) and algorithm B (red). The shaded areas contain the upper and lower quantiles ($n = 32$) and the dashed lines indicate the values of α yielding the optimal median RMSE between the true and estimated signals. The length N was set based on the optimal parameters in Table 4.1. An increased α led to increased variability, but the optimal α (dashed line) provided a good balance between median performance and variability.*

in the ΔSNR for both algorithms, indicating that a larger learning rate improves SNR more for some semi-synthetic signals while causing a reduced improvement for others. For some parameter values, the ΔSNR also took on *negative* values, meaning that the algorithms actually induced more artifact noise into the signal than what was effectively removed. This was especially prominent for algorithm B, which displayed an overall larger performance variation. A typical example of such a situation is show in Figure 4.2 where the artifact energy is considerably lower than the energy of the true EMG signal, causing the SNR between the true signal and the residual artifact (SNR_{out} in Eq. 3.8) to be larger than the SNR on the input (SNR_{in}), and thus yielding a negative ΔSNR.

By comparing the ΔSNR curves with the dashed lines representing the optimal parameter value for minimizing the median RMSE, it is evident that the two performance metrics were seemingly well correlated. The optimal parameters generally provided a sound trade-off between the median and lower quartile SNR improvement. As an example, consider the performance of algorithm A (blue) for the supinate channel (lower right) in Figure 4.1. By purely optimizing median ΔSNR, the optimal parameter would be $\alpha \approx 0.04$ which would yield a larger ΔSNR vari-

ability and even cause the lower quartile to lie below zero. Instead, the RMSE optima provided similar median and upper quartile ΔSNR performance, but with a considerably higher lower quartile.

In summary, an increased learning rate α led to increased performance variability and optimizing for RMSE provided a good balance between median performance and variability. Furthermore, a too high learning rate caused negative ΔSNR improvement, indicating that α needs to be tuned sufficiently low for correct functionality, especially for algorithm B.

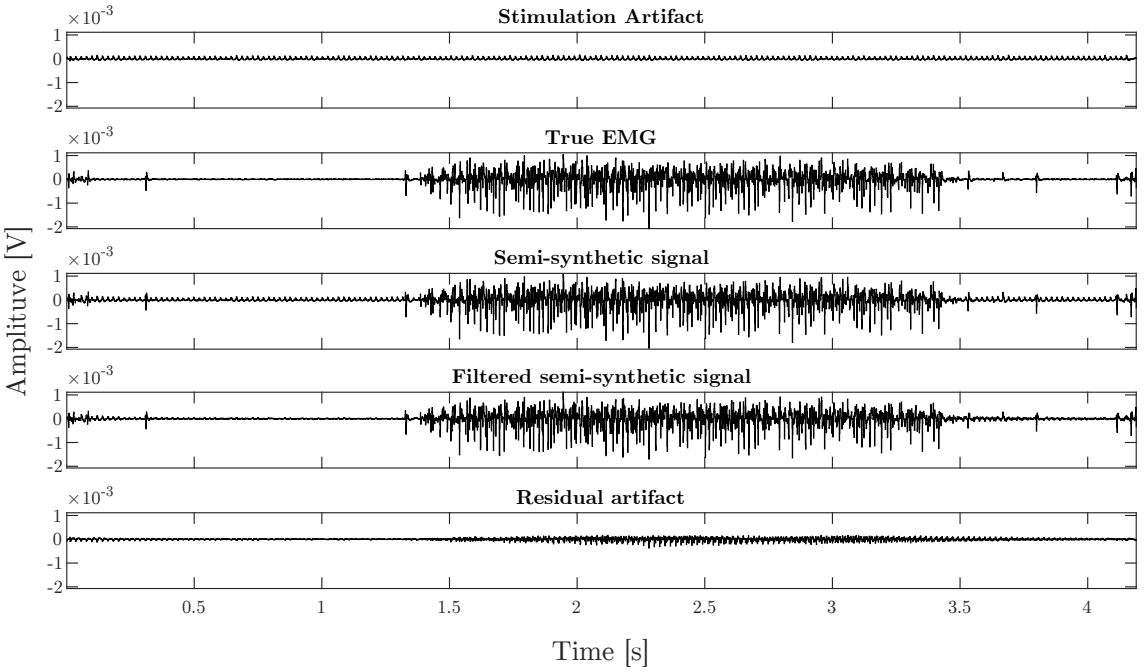

Figure 4.2: *Example of a semi-synthetic signal where the SNR on the input was higher than the SNR on the output yielding a negative ΔSNR of -1.52 dB. The signal was recorded on the close channel with stimulation at 50 Hz and pulse width and amplitude of $150\,\mu s$ and $450\,\mu A$, respectively. The semi-synthetic signal was filtered with algorithm A using the optimal hyperparameters from Table 4.1.*

Template/filter length

Considering the sensitivity when the template/filter length N was varied in Figure 4.3, the choice of N does not seem to be as crucial for determining the algorithms' performance as the learning rate. Specifically, increasing the length did not affect the SNR improvement in any major negative way, but rather seemed to yield an increased improvement.

One may observe that after a certain length the performance stayed constant. This is a logical behavior, considering that the number of samples between each stimulation pulse is dependent on the sampling and stimulation frequency. In the offline experiment, the semi-synthetic signals were sampled at 1000Hz and contained stimulation pulses generated at 30 and 50 Hz, leading to a maximum of roughly 33 samples between each pulse. It is therefore understandable that the algorithm performance

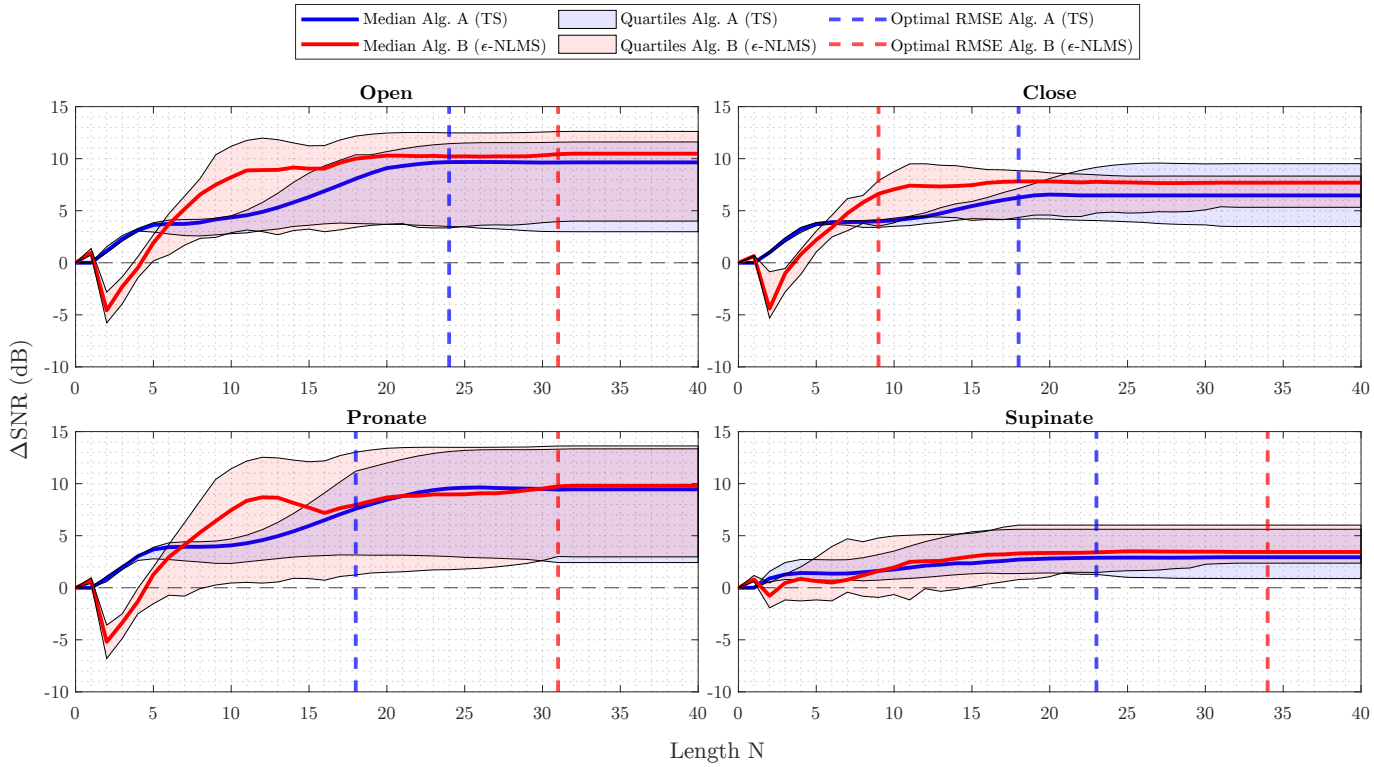

Figure 4.3: *Change in SNR per channel while varying the length N for algorithm A (blue) and algorithm B (red). The shaded areas contain the upper and lower quantiles ($n = 32$) and the dashed lines indicate the values of N yielding the optimal median RMSE between the true and estimated signals. The learning rate α was set based on the optimal parameters in Table 4.1. An increase in N improved performance for both algorithms, but algorithm B required a minimum length to provide a positive improvement while A caused immediate improvement starting from $N > 0$.*

stayed constant once $N \gtrapprox 30$ as both algorithms are reset to start over again once a new pulse is detected.

Another interesting observation is that algorithm A behaved similarly across all channels. When the template length was increased from zero, the SNR improvement was immediate and continued to increase when the template was extended. Considering algorithm B, however, a too short filter ($N \lessapprox 7$ in this case) actually decreased the SNR between the residual artifact and the true EMG signal when applying the algorithm rather than removing the stimulation artifact. It thus seems important that the filter length is chosen long enough to correctly reduce the artifact signal power.

In contrast to the learning rate, both algorithms' performance consistently improved as the template/filter length N increased. However, algorithm B required a sufficient length before any SNR improvement was noticed while algorithm A improved the SNR immediately when increasing the length from zero. This indicates that algorithm B requires more care when manually tuning the filter length. Optimizing for RMSE seemed to provide a reasonable trade-off between performance and

variability, although the observation was not as evident as for the learning rate.

4.3 Effect on control features

Figures 4.4, 4.5, 4.6, and, 4.7 present the violin plots with estimated densities for the four common features Mean Absolute Value (MAV), Zero Crossings (ZC), Slope Sign Changes (SSC), and Waveform Length (WL), respectively. By qualitatively examining the distributions, conclusions can be made about the stimulation artifact effects and how well the algorithms managed to reverse these effects.

In the optimal case, when the algorithms are able to completely remedy the effect of the stimulation artifacts, the distribution of feature values when applying either algorithm during stimulation (*S+A/B*) should be equal to the case without stimulation (*No S*) both in-between (blue) and during (red) EMG activity on each channel. Similarly, the pure effect of the stimulation can be seen by examining the difference in distribution between the no stimulation (*No S*) and stimulation only (*S*) cases, which for almost all features and channels change significantly.

Table 4.2 presents the resulting p-values from the Wilcoxon-Mann-Whitney hypothesis tests performed to examine if the feature value distributions during stimulation (*S*, *S+A* and *S+B)* were significantly different from the baseline case without stimulation (*No S*). As expected, most tests managed to reject the null hypothesis that the distributions were the same in favor of the alternative that they were not. There was, however, a slight trend that fewer distributions were significantly different when either of the two algorithms were applied as compared to when they were not, which supports the observations from the visual inspection of the distributions.

The rest of this section contains a short interpretation of the distribution differences for each of the four common features in relation to the violin plots.

Table 4.2: *p-values for Wilcoxon-Mann-Whitney U-test for different distributions between the No S and S, S+A, and S+B, respectively, for each feature, channel, and the case without EMG activity (blue) and with EMG activity (red). Bonferroni correction with a factor of 48 was applied. Gray background indicates statistically different distributions at significance level $\alpha = 0.05$ after correction.*

		No EMG activity (blue)			With EMG activity (red)		
	Channel	*No S / S*	*No S / S+A*	*No S / S+B*	*No S / S*	*No S / S+A*	*No S / S+B*
MAV	Open	0.000	>0.99	>0.99	0.000	>0.99	>0.99
	Close	0.000	0.040	0.555	0.000	0.000	0.000
	Pronate	0.000	0.001	>0.99	0.000	>0.99	>0.99
	Supinate	>0.99	0.000	0.000	0.000	0.000	0.000
ZC	Open	0.000	0.000	0.005	0.000	0.000	0.000
	Close	0.000	0.000	0.000	>0.99	>0.99	>0.99
	Pronate	0.000	0.000	0.000	0.000	0.000	>0.99
	Supinate	0.468	0.000	0.000	0.000	0.000	0.000
SSC	Open	0.000	0.679	0.000	0.000	0.000	0.001
	Close	0.000	0.000	0.487	>0.99	>0.99	>0.99
	Pronate	0.000	0.000	0.001	0.000	>0.99	>0.99
	Supinate	0.000	0.000	0.000	0.000	0.000	0.000
WL	Open	0.000	>0.99	>0.99	>0.99	0.015	>0.99
	Close	>0.99	0.192	>0.99	0.000	0.000	0.000
	Pronate	0.000	0.068	0.100	0.132	0.002	0.184
	Supinate	0.000	0.000	0.000	0.000	0.000	0.000

Mean Absolute Value

As can be seen in Figure 4.4, the effect of the two algorithms on the MAV feature was especially favorable for the open and pronate channels. The expected increase in MAV during stimulation was corrected by both algorithms, indicating that they are able to correctly remove the artifacts from the contaminated signals. Most notably was the case when no EMG activity was present on the channels (blue) where the stimulation caused a distribution shift that could easily be interpreted as EMG being active on the channel. The algorithms thus seem to prevent erroneous detection of EMG activity, which is especially important in the case of direct control where the MAV feature is the sole indicator of movement intent [13].

This observation was also supported by the statistical tests in Table 4.2 where the distributions during EMG activity were no longer significantly different after applying either algorithm. With no EMG activity, the same was true for algorithm B, but algorithm A did not completely correct the distribution on the pronate channel.

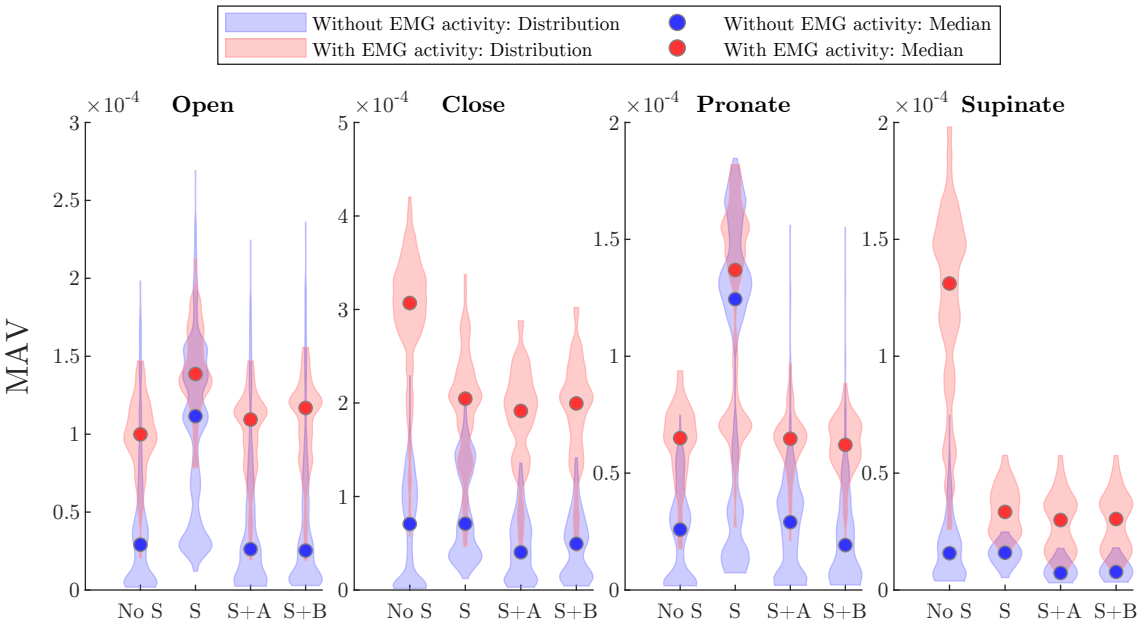

Figure 4.4: *Per-channel MAV feature value distributions during EMG contraction (red) and without EMG contraction (blue) in the case without any stimulation (No S), with stimulation (S), with stimulation and applying algorithm A (S+A), and with stimulation and applying algorithm B (S+B). For open and pronate channels, the distributions were more similar to the case without stimulation (No S) when algorithm A and B were applied (S+A and S+B, respectively), while the close and supinate channels exhibited no noticeable improvement.*

For the close and supinate channels, however, an interesting observation could be made. The MAV value during EMG activity was considerably *lower* during stimulation, regardless of whether any of the algorithms were applied or not. Assuming that the participant provided approximately constant level of contraction throughout the entire experiment, this suggests that the stimulation also has other fundamental effects on the signal acquisition circuitry, causing reduced signal amplitude or amplifier

sensitivity during stimulation. Such an effect is not easily reversed by any of the proposed algorithms, as these focus on removing the stimulation artifact waveform from the acquired signal and cannot directly address any effects that also apply to the actual EMG content of the signal. As expected, the statistical test showed significantly different distributions on both channels in all cases, except when applying algorithm B on the close channel without any present EMG activity.

Comparing the two algorithms against each other, it is evident that both resulting distributions agreed well with each other. One might therefore say that they perform equally well with respect to the MAV feature, even though the statistical test favored algorithm B slightly.

Zero Crossings

For the ZC features in Figure 4.5, the effect of applying the two algorithms varied greatly between each channel. On the open channel, applying the algorithms shifted the feature value distributions in the direction of the *No S* case, making the distributions more similar to each other but still significantly different according to the statistical test. The effect on the close channel was more subtle, showing no statistically significant change during EMG activity and only small non-significant improvements when EMG was not active, especially for algorithm A.

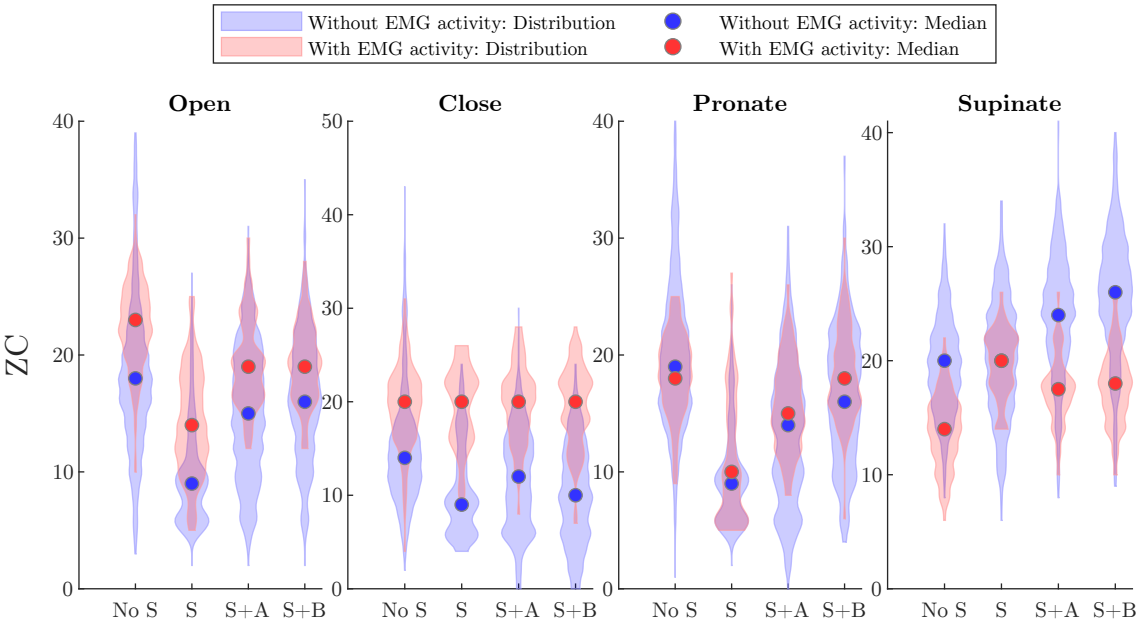

Figure 4.5: *Per-channel ZC feature value distributions during EMG contraction (red) and without EMG contraction (blue) in the case without any stimulation (No S), with stimulation (S), with stimulation and applying algorithm A (S+A), and with stimulation and applying algorithm B (S+B). Both the open and pronate channel showed noticeable improvement after applying either algorithm (S+A and S+B). Furthermore, the distribution overlap caused by stimulation (S) on the supinate channel was reverted by both algorithms at the cost of slight shift in the positive direction.*

Considering the pronate channel, algorithm B yielded distributions more similar to the *No S* case, but neither algorithm managed to revert the shift in relative ordering of the medians induced by the stimulation. According to the statistical test, however, the distribution from algorithm B during EMG activity was correctly recovered and no longer significantly different to the baseline case.

On the supinate channel, both algorithms moved the distribution of feature values away from the baseline (*No S*) regardless if any EMG activity was present or not and therefore actually worsened the similarities to the baseline case. This observation agreed with the result from the statistical test. On the other hand, the distribution overlap seen in the case without any algorithm (*S*) was almost completely remedied by the algorithm application. This suggests improved separability and most likely enhanced pattern recognition performance.

Slope Sign Changes

By studying the distribution of the SSC features, as shown in Figure 4.6, one observes that the stimulation seems to induce a decrease in SSC feature value, especially when no EMG activity is present on the channel (blue). This observation was supported by the statistical tests, showing significantly different distributions when comparing the baseline and the stimulation case on all channels. On the open, close, and pronate channels, this reduction was remedied by the application of either algorithm, although some distributions were still significantly different. The same was true for the supination channel, but here the algorithms also seemed to generally increase the

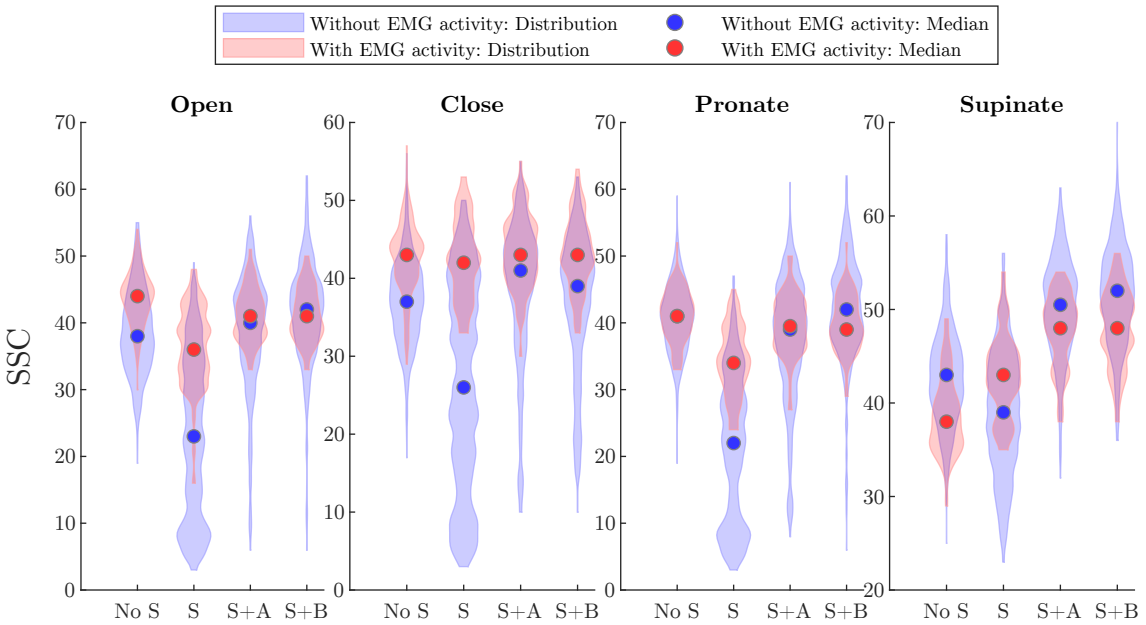

Figure 4.6: *Per-channel SSC feature value distributions during EMG contraction (red) and without EMG contraction (blue) in the case without any stimulation (No S), with stimulation (S), with stimulation and applying algorithm A (S+A), and with stimulation and applying algorithm B (S+B). Stimulation (S) generally caused a decrease in SSC value, especially when no EMG activity was present (blue), but the change was largely reverted by applying either algorithm.*

feature value also in the case of EMG activity being present (red), as well as restore the relative relation between the two cases' medians. This caused all distributions to remain significantly different according to the statistical test, regardless of algorithm application or EMG activity presence.

Comparing the two algorithms against each other, one notices that algorithm A generated slightly more similar feature value distributions to the baseline as compared to algorithm B. The difference was however minimal, and suggests that both algorithms perform similar with respect to the SSC features.

Waveform Length

Not surprisingly, the WL features in Figure 4.7 behaved much like the MAV features in Figure 4.4. For the open and pronate channels, the algorithms' effects were most noticeable in a general reduction of feature value. However, the reduction seemed larger when EMG activity was not present (blue), which caused the distributions to be more similar to the baseline (*No S*) than when no algorithm was applied (*S*). Considering the statistical test, both algorithms yielded distributions that were not statistically different when no EMG activity was present. During EMG activity, however, algorithm A caused distributions that were not significantly different during stimulation to be different after application, which was not observed for algorithm B.

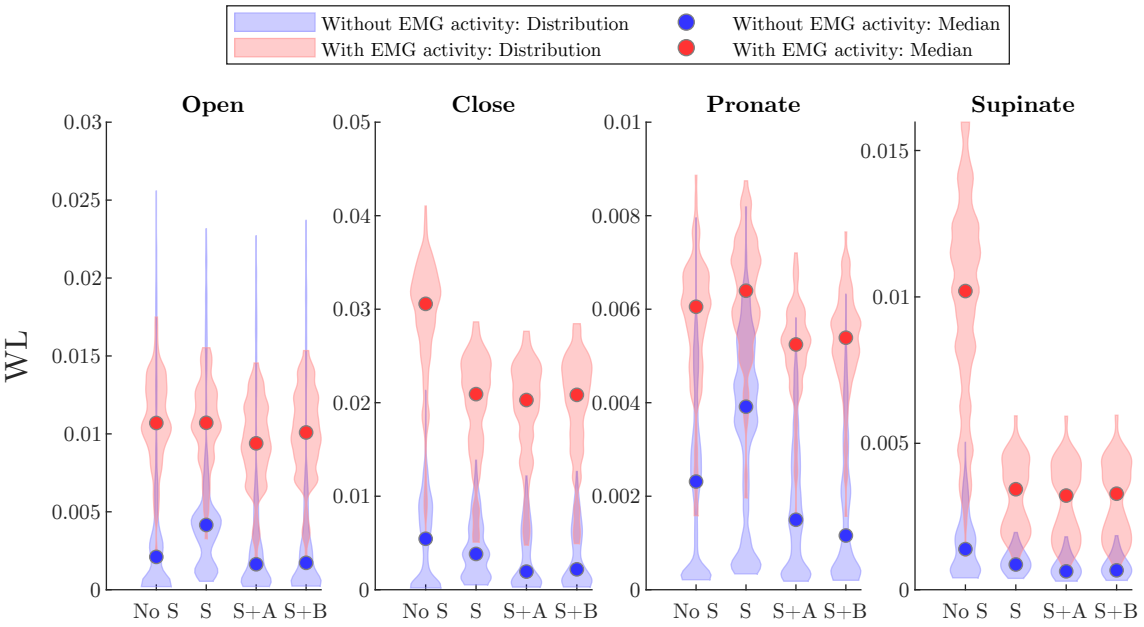

Figure 4.7: *Per-channel WL feature value distributions during EMG contraction (red) and without EMG contraction (blue) in the case without any stimulation (No S), with stimulation (S), with stimulation and applying algorithm A (S+A), and with stimulation and applying algorithm B (S+B). For open and pronate channels, the distributions were more similar to the case without stimulation (No S) when algorithm A and B were applied (S+A and S+B, respectively), while the close and supinate channels exhibited no noticeable improvement.*

As with the MAV feature, even though there was a slight shift towards lower feature values when the algorithms were applied, the effect on the close and supinate channels was negligible and also confirmed by the statistical test. The same phenomenon, where the feature values decreased significantly during stimulation was also observed, which was to be expected given that both WL and MAV are highly affected by signal amplitude. Similarly, the two algorithms seemed have an general equal effect on the SSC feature value distributions.

Summary
In summary, the stimulation generally led to an increase in MAV and WL feature values, except for on the close and supinate channels where the overall signal amplitude was unexpectedly decreased during stimulation. For the open and pronate channels, however, both algorithms were able to correct the increased values and return the distributions to roughly the same level as when no stimulation was applied.

The effect on the ZC feature values varied greatly between channels. Both open and pronate channels exhibited a shift towards lower feature values during stimulation, and applying the algorithms generally improved the situation. The close channel saw a similar change during stimulation when no EMG activity was present, but no significant difference during EMG activity. On the supinate channel, the overlap in distribution caused by stimulation was reduced at the cost of generally increased feature values.

For the SSC feature, the stimulation generally caused decreasing values, especially when there was no EMG activity on the channel. On all channels except the supinate channel, both algorithms showed a positive effect on the SSC distributions, and were able to restore them almost entirely. On the supinate channel, the distribution medians were reordered during stimulation, but the change was reverted by both algorithms at the cost of a positive shift in feature values.

4.4 Online evaluation

Figure 4.8 presents the MAV feature values resulting from the preliminary online evaluation. As expected, the feature distributions look similar to those reported for the offline experiment, although a few differences can be observed. On all channels, the stimulation (S) caused a general increase in MAV feature values as compared to the baseline ($No\ S$). The same overall decrease in signal amplitude on the close and supinate channels was also observed, although the EMG amplitude in relation to the stimulation artifact on the supinate channel seemed small than during the offline experiment. On all channels, most of the effect of the stimulation artifacts was reverted by the application of each algorithm, especially when no EMG activity was present. Furthermore, no significant difference in performance between the two algorithms was noticed.

An interesting observation regarding the EMG signals was however made. At the start of each stimulation period of manually activating the stimulation feedback, an extra large signal spike with different shape compared to the regular artifacts was observed on all channels. This was reflected in the narrow spikes of larger MAV

feature values seen in Figure 4.8, and was most likely induced by the stimulation circuitry.

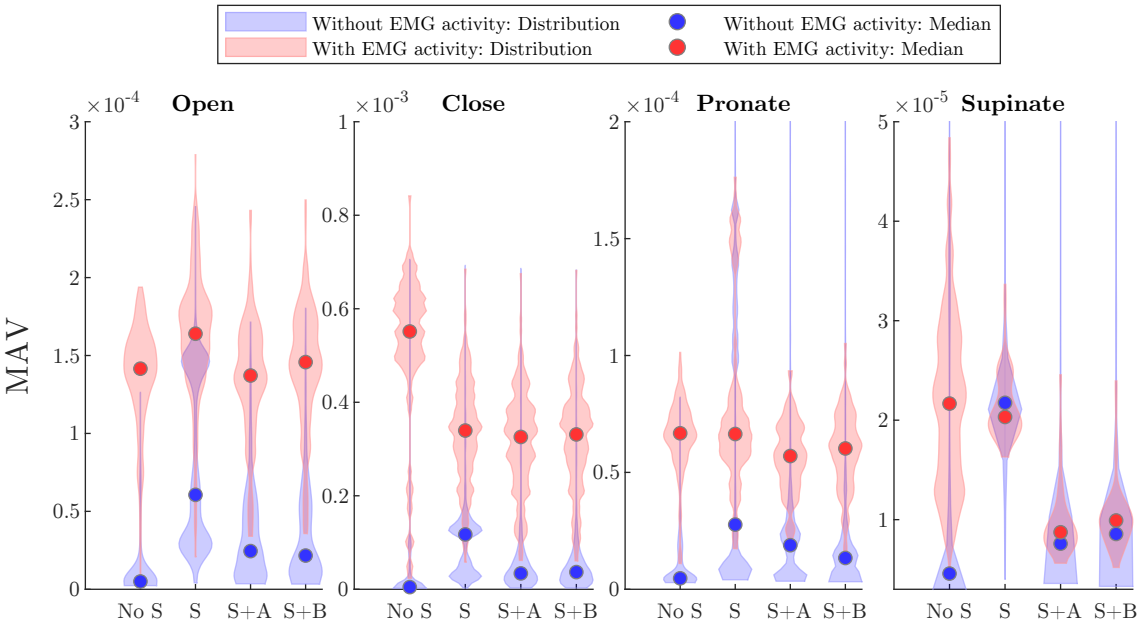

Figure 4.8: *Per-channel MAV feature value distributions from the preliminary online experiment during EMG contraction (red) and without EMG contraction (blue) in the case without any stimulation (No S), with stimulation (S), with stimulation and applying algorithm A (S+A), and with stimulation and applying algorithm B (S+B). For all channels, the distributions were more similar to the case without stimulation (No S) when algorithm A and B were applied (S+A and S+B, respectively), when no EMG activity was present. The close and supinate channel exhibited an unrecoverable decrease in signal amplitude during stimulation.*

5

Discussion

This chapter contains a discussion of the chosen methodology including the experimental setup, algorithm choice and design, selection of evaluation metrics, and their limitations. The most important results are reiterated to answer the research questions and a short mention about sociological and ethical aspects in relation to this research is given.

5.1 Results

Hyperparameters
Results on the lowest achievable RMSE during the parameter optimization indicate that algorithm B performs slightly better than algorithm A.

Considering the algorithms' sensitivity to variations in the two hyperparameters α and N, the results suggest that an increase in the learning rate α generally leads to higher variability with increased performance for some semi-synthetic signals and worsened performance for others. The increased variability additionally led to a negative ΔSNR caused by more noise being introduced in the signal than what was removed in terms of artifacts. On the other hand, optimizing the RMSE seemed to provide a good balance between median performance and performance variability, suggesting that the RMSE is a useful optimization metric for automatic selection of hyperparameters.

Neither algorithm was negatively affected by an increase in the length parameter N, but the improvement was constant once the inter-pulse period was reached. Additionally, algorithm B required a sufficient filter length ($N \gtrapprox 7$) to yield improvements in SNR, while algorithm A provided a consistent improvement starting from $N = 1$. This indicates that algorithm B, based on the ϵ-NLMS adaptive filter, is dependent on a sufficient number of previous samples on the reference channel to be able to predict the artifact waveform correctly. Furthermore, algorithm A seems to require a larger N to reach the same performance as algorithm B.

Given the two algorithms' different approaches to predicting the artifact, this behavior is expected. Algorithm A's approach of constructing a template for each of the N samples following the stimulation pulse, naturally requires a large enough N depending on the length of the artifact in the time domain for enough effect. On the other hand, when basing the prediction on the N last samples, as in algorithm B, a lower but large enough N is sufficient to adequately predict the artifact.

Effect on control features
Examining the effect on the four common features used for myoelectric pattern recognition, the stimulation generally led to an increase in MAV and WL feature values, except for on the close and supinate channels where the overall signal amplitude was unexpectedly decreased during stimulation. For the open and pronate channels, however, both algorithms were able to correct the increased values and return the distributions to roughly the same level as when no stimulation was applied.

The effect on the ZC feature values varied greatly between channels. Both open and pronate channels exhibited a shift towards lower feature values when stimulation was enabled, but applying the algorithms generally improved the situation. The close channel saw a similar change during stimulation when no EMG activity was present, but no significant difference during EMG activity. For the supinate channel, enabling stimulation caused the feature value distributions to overlap almost completely, but by applying either algorithm, this overlap was reduced at the cost of generally increasing feature values as compared to the baseline case without stimulation.

For the SSC feature, the stimulation generally caused decreasing values, especially in the case when there was no EMG activity on the channel. On all channels except the supinate channel, both algorithms showed a positive effect on the SSC distributions, and were able to restore them almost entirely. The effect on the features on the supinate channel was somewhat different, causing the distribution medians to change their relative ordering. By applying the algorithms this change was reverted, but the feature values were instead shifted further into the positive direction.

Even though neither algorithm provided a perfect solution to the problem of stimulation artifacts affecting the feature values, the feature value distributions generally improved to have similar shape and location to those when no stimulation was applied at all. This illustrates both algorithms' possibilities of improving pattern recognition performance when the pattern recognition was not previously trained to support these situations. Additionally, the algorithms provided improved distribution separability between the active and not active case, and as such would most likely also positively impact pattern recognition performance even when feature values from processed signals are included during training. The positive improvements on the distribution on MAV feature values also suggest the two algorithms' applicability when using direct control.

However, it is worth keeping in mind that an improved signal and feature value distribution, due to the application of either algorithm, does not automatically imply improved prosthesis usability. Thus, further studies involving real pattern recognition performance and functional prosthesis tests are suggested to investigate actual implication for usability and reliability.

Algorithm Comparison
When comparing the two algorithms, there is no clear evidence supporting that one is significantly better than the other. In the evaluation of the algorithms' sensitivity to variations in the hyperparameters, both algorithms performed similarly in terms

of achieved SNR improvement. Algorithm B, however, seemed to require more care when selecting parameters since a too high learning rate α quickly degraded the lower quartile performance and a too low filter length N induced more noise in the signal, ultimately causing a negative SNR improvement. In this respect, algorithm A, which had a larger range of values of α that provided sufficient performance and showed consistent performance increase for all values of N, gives the impression of being easier to tune manually. On the other hand, algorithm B achieved a lower RMSE reconstruction error during hyperparameter optimization.

When considering the effect on the feature value distributions, neither algorithm A nor B performed consistently better than the other, although the results of the statistical test favored algorithm B slightly.

On the theoretical side, especially regarding computational complexity, algorithm A has an overall lesser impact as it only requires a few additions and two multiplications for each sample, while algorithm B relies on costly inner products with vectors of length N. These inner products are essentially performing a convolution with the filter weights, and can be considered a generally costly operation. In addition to the N floating-point filter weights required by both algorithms, algorithm B also requires storing N floating-point values for the previous reference sample values, causing a doubled memory usage for the same value of N. However, as seen in the optimization results, algorithm B can provide better performance with a much lower filter length for some channels, and thus the difference in memory usage might be of less importance.

Furthermore, the adaptive filter foundation of algorithm B has the opportunity to generalize to varying artifacts caused by modulated stimulation parameters as it relies on the reference, which is assumed to be highly correlated with the SA itself. Modulated stimulation was not studied in this thesis, however, and is thus a topic for continued investigation.

Inter-channel variations
As seen from the findings in this thesis, the behavior, both in terms of algorithm performance and stimulation artifact influence, varied greatly between each channel. Considering the anatomy of the human body, this is not an unexpected observation. The fact that the recording electrodes are placed in different locations relative to the stimulation electrode and are located on muscles of varying size and myoelectric behavior, naturally implies that some electrodes are more susceptible to interference from stimulation artifacts than others. This motivated the choice of optimizing the parameters for each channel individually, and further suggests that the choice of algorithm and hyperparameters and the resulting performance needs to be considered on a per-channel basis and not necessarily on a per-participant basis. Therefore, rather than providing a definite answer to the question of how to mitigate the effect of stimulation artifacts, the work in this thesis provides additional tools and insights for dealing with the problem.

Real-time performance
As expected, the preliminary online evaluation showed similar results as compared to the initial offline evaluation. Only the MAV features were considered, however,

which greatly limits the power of any real-time algorithm performance findings. Nevertheless, the fact that both algorithms were able to process the acquired samples in real-time suggests that they are suitable for real-time operation on the embedded controller.

The observation of the larger spike in the beginning of each stimulation pulse train also indicate that more development is needed to, e.g., blank the first pulse in each train during more samples.

5.2 Methodology

Experimental setup
The goal of the performed experiment was to collect EMG signals both with and without stimulation and EMG activity. This was performed with the help of a hardware platform designed and used for myoelectric prosthesis control, which was also the intended platform for implementation of the chosen algorithms. The signals were recorded from one participant with transhumeral (above-elbow) amputation who had been a daily prosthesis user for over two years. Thus, the recorded signals are considered typical for use in myoelectric control of a prosthesis device and therefore align with the aim of this thesis.

The inclusion of only one participant in the study, however, greatly limits the power of the general findings.Future studies including more participants are therefore recommended to extend and validate the knowledge and conclusions from this thesis.

Algorithm selection
The algorithm selection step was based on a study of previous work on artifact removal in general and stimulation artifact removal in particular. As the existing literature on removing stimulation artifact caused by implanted electrodes, both recording and stimulation ones, was scarce, it was assumed that algorithms that performed well in other situations, for example using surface electrodes, could also work in the context of this thesis. As such, two algorithms with promising previous usage together with implementation simplicity and low overall computational complexity were chosen.

The option of choosing algorithms based on component decomposition was excluded based on the high computational cost and more complicated mathematical implementation. This was further motivated by the ease of implementation by other algorithms, such as those that were ultimately selected, especially considering the computational limitations and the availability of a reference and stimulation synchronization signal on the hardware platform. However, as the decomposition methods often provide better resulting performance [10], and that methods such as DWT have been successfully used for signal filtering and denoising in an embedded system [47], [48], they are still worth considering on a system-wide perspective. This is especially true if artifact removal, filtering, and denoising steps could be combined with feature extraction to only require a single decomposition stage to facilitate them all. The feasibility of this approach remains an open question suitable for further investigation.

Two limitations that both chosen algorithms exhibit is that they rely on the assumption that the stimulation artifact is additive with respect to the underlying EMG signal. Given that the body is a complex volume conductor, it is fair to expect such an assumption to not hold entirely. For example, considering the general decrease in signal amplitude observed in Figure 4.4 and assuming that the level of EMG contraction elicited by the experiment participant was constant, it is clear that the stimulation does not always only have an additive affect on the underlying signal. In this case, the stimulation also affected the actual recording circuitry which additionally changed the recorded EMG signal waveform and could not be corrected by any of the implemented algorithms.

Furthermore, algorithm B is based on an adaptive filter that additionally assumes a linear relationship between the reference signal and the stimulation artifact. The choice of reference is thus critical and by utilizing the samples acquired from the stimulation electrode directly, naturally some of the nonlinear relationships due to the volume conducting body can be incorporated into the reference. Contrasting that with using a simple unit pulse for symbolizing the stimulation pulse, such as the synchronization signal available on the hardware platform, the approach employed here is thus less likely to suffer from the restriction of a linear relationship. To further explore the relation between the reference and the artifact, methods such as the one presented by Grieve *et al.* [40] could be considered for future investigation. Granted that the computational complexity can be kept at an appropriate level, the relation might be more appropriately modeled by a MLP rather than by a direct linear mapping as used here.

Another limitation of both algorithms is that they work on a sample-by-sample basis. Each new sample is thus only filtered based on the information contained in the previous samples. This makes implementation simple and the computational complexity can be spread out over each sample acquisition, instead of all samples being processed after each sample window during the feature extraction step. However, this also means that information about future samples is not taken into account by any of the algorithms, information that could potentially prove useful and improve performance.

Optimization procedure

The optimization procedure relied on the median of the RMSE between the true and estimated signals as the optimization objective. From a control perspective, using the median is reasonable as the goal is to optimize for the general better performance, while allowing some combinations of stimulation parameters and EMG signals to give worse performance. On the other hand, this means that the hardest cases are not taken into account, potentially missing cases that could be avoided if considered during optimization. The median is also not a continuous function, compared to the mean, which makes the optimization problem more difficult.

The choice of optimization metric is also a point for further investigation. Even though optimizing the RMSE is a natural choice when aiming to reconstruct the original signal optimally and here seemed to provide a good balance between median performance and performance variability, other metrics might also be worth

considering depending on the specific purpose. For example, with the goal to directly improve the effect on the feature value distributions, using metrics that measure cluster/distribution similarity and/or separability might prove beneficial. With focus on prosthesis controllability, the objective could also be based on pattern recognition accuracy/performance directly.

Another limitation of the chosen optimization procedure is the lack of a scheme for avoiding overfitting the hyperparameters to the semi-synthetic signals, potentially lowering generalizability. Instead of blindly optimizing the hyperparameters based on the RMSE errors for *all* semi-synthetic signals at the same time, one could leave one or a few of the signals out while optimizing the parameters for the rest. Those parameters could then be used to measure the objective on the held-out signals, and thus provide information about the ability to apply the algorithms with those parameters on previously unseen signals.

Evaluation
Evaluation of the performance of the two algorithms was performed in terms of SNR improvement on the semi-synthetic signals and changes in feature value distributions during stimulation. As the SNR depends on the relative energy of the artifact and the signal, it is directly related to the reduction of artifact components in the signal. It therefore provides a metric with higher interpretability than the RMSE used for the optimization procedure and other metrics such as the correlation coefficient [28] previously employed to measure artifact removal performance.

The changes in feature value distributions were evaluated by visual inspection and using statistical tests to indicate significance in distribution differences. This provided an initial indication of the stimulation effect and algorithm applicability, especially for direct control using the MAV features, but is limited by the fact that the distributions from each channel and feature type were considered separately and not together. Thus, the effect on actual class-conditional distributions for each movement, as often used for pattern recognition, was not studied. To further investigate how the feature values vary together, future work could therefore investigate actual pattern recognition performance or use high-dimensional clustering and dimensionality reduction techniques to evaluate distribution changes.

As the Wilcoxon-Mann-Whitney U-test used for testing significant distribution differences is a non-parametric test, it was well suited for application in this thesis since the feature values not necessarily follow any specific distribution. Considering the Bonferroni correction applied to correct for multiple comparisons and control the family-wise error rate, more involved approaches with increased power, such as Holm-Bonferroni correction [54], could be used in future work. Nonetheless, for the initial development and analysis performed in this thesis, the simple Bonferroni correction was considered sufficient.

5.3 Sociological and ethical considerations

The ethical considerations of the work in this thesis are the same as in the development of any medical device. Thus thorough testing, verification and ethical approval is required before the technology can be approved for general use. The experiments in this thesis were covered by an already approved ethical application, and thus no further amendment was required. Furthermore, the hardware platform was already tested and approved for use in this context, and the implemented algorithms will require similar extensive testing before being allowed for everyday use.

Although the artifact removal algorithms cannot put the prosthesis user at any direct risk, they can ultimately alter the usability and function of the prosthesis device while processing the signals used for control. On the other hand, the fact that the work here was specifically performed using a prosthetic arm limits the risks for the prosthesis user. Compared to a prosthetic leg, where malfunctioning or erroneous control could be fatal in terms of user injuries, the loss of control of a prosthetic arm is less likely to lead to severe injuries and risk. Nevertheless, the consideration of degraded performance was taken into account during algorithm selection to exclude high-risk methods in favor of simple and effective algorithms. The result of the evaluation also indicated that both algorithms could be tuned manually without considerable risk for degraded signal quality.

From a sociological perspective, the development of a prosthesis device is always associated with questions regarding availability and daily life implications. Previous research on the highly integrated e-OPRA system has shown to have positive effects on self-esteem, self-image and social interactions directly linked to the enhanced prosthesis functionality and use in daily living [55]. By developing algorithms for artifact removal to restore control during neurostimulation, additional users could benefit from sensory feedback while wearing their prosthesis in daily life. On the other hand, the use of such development devices often means that the prosthesis user is dependent on the researcher to get access to the technology.

Nevertheless, apart from the risk of reduced control, the work in this thesis is not considered to involve any significant ethical consequences, but rather provide opportunities for improved prosthesis functionality.

6

Conclusion

The purpose of this thesis was to investigate, implement, and evaluate algorithms for removing stimulation artifacts from EMG control signals in real-time on an embedded prosthesis controller. By examining previous literature on the topic of stimulation artifact removal and performing experiments where EMG signals containing stimulation artifacts were recorded from one participant with a transhumeral amputation using an osseointegrated prosthesis in daily life, two algorithms were implemented and evaluated. The two algorithms were based on the TS and ϵ-NLMS approaches, and evaluated in terms of their ability to correct changes in the distribution of four signal features commonly used for myoelectric pattern recognition.

The experiments and evaluation confirmed that the suggested algorithms were able to revert and/or improve the changes induced by the stimulation artifacts, although the extent varies notably between each EMG channel. Furthermore, both algorithms performed similar, but investigations of sensitivity to parameter settings indicate that the algorithm based on TS might be easier to use during manual tuning. On two channels, a phenomenon of general signal amplitude decrease during stimulation was observed, which could not be remedied by either algorithm and can most likely be attributed hardware effects.

The algorithms were also preliminary evaluated online in real-time by implementation on the hardware platform. Even though the results were not as conclusive as the offline observations, both algorithms were able to operate for all channels in real-time and thus hold promise for future applications.

Despite not evaluating actual pattern recognition performance, the findings suggest that both algorithms can prove useful in alleviating the negative effects on myoelectric pattern recognition during stimulation to improve prosthesis control and usability. In turn, this would further allow neurostimulation to be used for enhancing tactile feedback for prosthesis users.

The large inter-channel variation can most likely be attributed to the individual recording and stimulation electrode arrangements, and sheds light on the fact that finding a general solution to the problem of stimulation artifacts is considerably difficult. However, despite its exploratory nature and only being based on data from one participant, this thesis provides insights and tools for dealing with such artifacts in real-time on embedded hardware.

Further research could usefully explore the immediate implications for prosthesis control by including functional tests and more participants. Furthermore, inves-

tigations into combining signal processing and feature extraction stages to utilize a single signal decomposition step and make the approach more justifiable on the embedded hardware could also prove useful, as this is an area that has not yet seen much development.

References

[1] K. Ziegler-Graham, E. J. MacKenzie, P. L. Ephraim, T. G. Travison, and R. Brookmeyer, "Estimating the Prevalence of Limb Loss in the United States: 2005 to 2050," *Archives of Physical Medicine and Rehabilitation*, vol. 89, no. 3, pp. 422–429, Mar. 2008. DOI: 10.1016/j.apmr.2007.11.005.

[2] A. A. S. LLC, *Amputee Statistics You Ought to Know | AdvancedAmputees.com*, 2012.

[3] M. Zheng, M. Crouch, and M. S. Eggleston, "Surface Electromyography as a Natural Human-Machine Interface: A Review," Jan. 2021.

[4] T. A. Kuiken, G. A. Dumanian, R. D. Lipschutz, L. A. Miller, and K. A. Stubblefield, "The use of targeted muscle reinnervation for improved myoelectric prosthesis control in a bilateral shoulder disarticulation amputee," *Prosthetics and Orthotics International*, vol. 28, no. 3, pp. 245–253, 2004. DOI: 10.3109/03093640409167756.

[5] M. Ortiz-Catalan, B. Håkansson, and R. Brånemark, "An osseointegrated human-machine gateway for long-term sensory feedback and motor control of artificial limbs," *Science Translational Medicine*, vol. 6, no. 257, pp. 6–257, Oct. 2014. DOI: 10.1126/scitranslmed.3008933.

[6] *Upgrade your OPRA Implant System to e-OPRA*, 2019.

[7] E. Mastinu, R. Branemark, O. Aszmann, and M. Ortiz-Catalan, "Myoelectric signals and pattern recognition from implanted electrodes in two TMR subjects with an osseointegrated communication interface," in *Proceedings of the Annual International Conference of the IEEE Engineering in Medicine and Biology Society, EMBS*, vol. 2018-July, Institute of Electrical and Electronics Engineers Inc., Oct. 2018, pp. 5174–5177. DOI: 10.1109/EMBC.2018.8513466.

[8] M. Ortiz-Catalan, E. Mastinu, P. Sassu, O. Aszmann, and R. Brånemark, "Self-Contained Neuromusculoskeletal Arm Prostheses," *New England Journal of Medicine*, vol. 382, no. 18, pp. 1732–1738, Apr. 2020. DOI: 10.1056/nejmoa1917537.

[9] C. Hartmann, S. Došen, S. Amsuess, and D. Farina, "Closed-loop control of myoelectric prostheses with electrotactile feedback: Influence of stimulation artifact and blanking," *IEEE Transactions on Neural Systems and Rehabilitation Engineering*, vol. 23, no. 5, pp. 807–816, Sep. 2015. DOI: 10.1109/TNSRE.2014.2357175.

[10] A. Zhou, B. C. Johnson, and R. Muller, *Toward true closed-loop neuromodulation: artifact-free recording during stimulation*, Jun. 2018. DOI: 10.1016/j.conb.2018.01.012.

[11] S. R. Devasahayam, "The Electromyogram," in *Signals and Systems in Biomedical Engineering*, Boston, MA: Springer US, 2013, pp. 253–279. DOI: 10.1007/978-1-4614-5332-1{_}11.

[12] A. D. Roche, H. Rehbaum, D. Farina, and O. C. Aszmann, "Prosthetic Myoelectric Control Strategies: A Clinical Perspective," *Current Surgery Reports*, vol. 2, no. 3, 2014. DOI: 10.1007/s40137-013-0044-8.

[13] E. Scheme and K. Englehart, "Electromyogram pattern recognition for control of powered upper-limb prostheses: State of the art and challenges for clinical use," *Journal of Rehabilitation Research and Development*, vol. 48, no. 6, pp. 643–660, 2011. DOI: 10.1682/JRRD.2010.09.0177.

[14] B. Hudgins, P. Parker, and R. N. Scott, "A New Strategy for Multifunction Myoelectric Control," *IEEE Transactions on Biomedical Engineering*, vol. 40, no. 1, pp. 82–94, 1993. DOI: 10.1109/10.204774.

[15] C. Günter, J. Delbeke, and M. Ortiz-Catalan, *Safety of long-term electrical peripheral nerve stimulation: Review of the state of the art*, Jan. 2019. DOI: 10.1186/s12984-018-0474-8.

[16] M. Ortiz-Catalan, J. Wessberg, E. Mastinu, A. Naber, and R. Branemark, "Patterned Stimulation of Peripheral Nerves Produces Natural Sensations With Regards to Location but Not Quality," *IEEE Transactions on Medical Robotics and Bionics*, vol. 1, no. 3, pp. 199–203, Jul. 2019. DOI: 10.1109/tmrb.2019.2931758.

[17] K. T. Sweeney, T. E. Ward, and S. F. McLoone, "Artifact removal in physiological signals-practices and possibilities," *IEEE Transactions on Information Technology in Biomedicine*, vol. 16, no. 3, pp. 488–500, 2012. DOI: 10.1109/TITB.2012.2188536.

[18] E. A. Brown, J. D. Ross, R. A. Blum, Y. Nam, B. C. Wheeler, and S. P. DeWeerth, "Stimulus-artifact elimination in a multi-electrode system," *IEEE Transactions on Biomedical Circuits and Systems*, vol. 2, no. 1, pp. 10–21, Mar. 2008. DOI: 10.1109/TBCAS.2008.918285.

[19] B. C. Johnson, S. Gambini, I. Izyumin, A. Moin, A. Zhou, G. Alexandrov, S. R. Santacruz, J. M. Rabaey, J. M. Carmena, and R. Muller, "An implantable 700μW 64-channel neuromodulation IC for simultaneous recording and stimulation with rapid artifact recovery," in *IEEE Symposium on VLSI Circuits, Digest of Technical Papers*, Institute of Electrical and Electronics Engineers Inc., Aug. 2017, pp. C48–C49. DOI: 10.23919/VLSIC.2017.8008543.

[20] E. J. Peterson, D. A. Dinsmoor, D. J. Tyler, and T. J. Denison, "Stimulation artifact rejection in closed-loop, distributed neural interfaces," in *European Solid-State Circuits Conference*, vol. 2016-Octob, IEEE Computer Society, Oct. 2016, pp. 233–236. DOI: 10.1109/ESSCIRC.2016.7598285.

[21] S. Stanslaski, P. Afshar, P. Cong, J. Giftakis, P. Stypulkowski, D. Carlson, D. Linde, D. Ullestad, A. T. Avestruz, and T. Denison, "Design and validation of a fully implantable, chronic, closed-loop neuromodulation device with concurrent sensing and stimulation," *IEEE Transactions on Neural Systems and Rehabilitation Engineering*, vol. 20, no. 4, pp. 410–421, 2012. DOI: 10.1109/TNSRE.2012.2183617.

[22] D. T. O'Keeffe, G. M. Lyons, A. E. Donnelly, and C. A. Byrne, "Stimulus artifact removal using a software-based two-stage peak detection algorithm," *Journal of Neuroscience Methods*, vol. 109, no. 2, pp. 137–145, 2001. DOI: 10.1016/S0165-0270(01)00407-1.

[23] A. E. Hines, P. E. Crago, G. J. Chapman, and C. Billian, "Stimulus artifact removal in EMG from muscles adjacent to stimulated muscles," *Journal of Neuroscience Methods*, vol. 64, no. 1, pp. 55–62, Jan. 1996. DOI: 10.1016/0165-0270(95)00099-2.

[24] L. F. Heffer and J. B. Fallon, "A novel stimulus artifact removal technique for high-rate electrical stimulation," *Journal of Neuroscience Methods*, vol. 170, no. 2, pp. 277–284, May 2008. DOI: 10.1016/j.jneumeth.2008.01.023.

[25] U. Hoffmann, W. Cho, A. Ramos-Murguialday, and T. Keller, "Detection and removal of stimulation artifacts in electroencephalogram recordings," in *Proceedings of the Annual International Conference of the IEEE Engineering in Medicine and Biology Society, EMBS*, IEEE, 2011, pp. 7159–7162. DOI: 10.1109/IEMBS.2011.6091809.

[26] A. Zhou, S. R. Santacruz, B. C. Johnson, G. Alexandrov, A. Moin, F. L. Burghardt, J. M. Rabaey, J. M. Carmena, and R. Muller, *Wand: A 128-channel, closed-loop, wireless artifact-free neuromodulation device*, Aug. 2017.

[27] C. Waddell, J. A. Pratt, B. Porr, and S. Ewing, "Deep brain stimulation artifact removal through under-sampling and cubic-spline interpolation," in *Proceedings of the 2009 2nd International Congress on Image and Signal Processing, CISP'09*, 2009. DOI: 10.1109/CISP.2009.5301199.

[28] Y. Li, J. Chen, and Y. Yang, "A Method for Suppressing Electrical Stimulation Artifacts from Electromyography," *International Journal of Neural Systems*, vol. 29, no. 6, p. 1 850 054, Aug. 2019. DOI: 10.1142/S0129065718500545.

[29] I. Iturrate, M. Pereira, and J. d. R. Millán, *Closed-loop electrical neurostimulation: Challenges and opportunities*, Dec. 2018. DOI: 10.1016/j.cobme.2018.09.007.

[30] T. Keller and M. R. Popovic, "Real-time stimulation artifact removal in EMG signals for neuroprosthesis control applications.," *Proceedings of the 6th Annual IFESS Conference*, no. January 2014, pp. 4–6, 2001.

[31] M. Azin, H. J. Chiel, and P. Mohseni, "Comparisons of FIR and IIR implementations of a subtraction-based stimulus artifact rejection algorithm," in *Annual International Conference of the IEEE Engineering in Medicine and Biology - Proceedings*, 2007, pp. 1437–1440. DOI: 10.1109/IEMBS.2007.4352570.

[32] D. A. Wagenaar and S. M. Potter, "Real-time multi-channel stimulus artifact suppression by local curve fitting," *Journal of Neuroscience Methods*, vol. 120, no. 2, pp. 113–120, Oct. 2002. DOI: 10.1016/S0165-0270(02)00149-8.

[33] B. H. Boudreau, K. B. Englehart, A. D. Chan, and P. A. Parker, "Reduction of stimulus artifact in somatosensory evoked potentials: Segmented versus subthreshold training," *IEEE Transactions on Biomedical Engineering*, vol. 51, no. 7, pp. 1187–1195, Jul. 2004. DOI: 10.1109/TBME.2004.827342.

[34] A. H. Sayed, *Adaptive Filters*. John Wiley and Sons, Jan. 2008, pp. 1–786. DOI: 10.1002/9780470374122.

[35] B. Widrow, C. S. Williams, J. R. Glover, J. M. McCool, R. H. Hearn, J. R. Zeidler, J. Kaunitz, E. Dong, and R. C. Goodlin, "Adaptive Noise Cancelling: Principles and Applications," *Proceedings of the IEEE*, vol. 63, no. 12, pp. 1692–1716, 1975. DOI: 10.1109/PROC.1975.10036.

[36] N. V. Thakor and Y. S. Zhu, "Applications of Adaptive Filtering to ECG Analysis: Noise Cancellation and Arrhythmia Detection," *IEEE Transactions on Biomedical Engineering*, vol. 38, no. 8, pp. 785–794, 1991. DOI: 10.1109/10.83591.

[37] S. Basir-Kazeruni, S. Vlaski, H. Salami, A. H. Sayed, and D. Markovic, "A blind Adaptive Stimulation Artifact Rejection (ASAR) engine for closed-loop implantable neuromodulation systems," in *International IEEE/EMBS Conference on Neural Engineering, NER*, IEEE Computer Society, Aug. 2017, pp. 186–189. DOI: 10.1109/NER.2017.8008322.

[38] C. Marque, C. Bisch, R. Dantas, S. Elayoubi, V. Brosse, and C. Pérot, "Adaptive filtering for ECG rejection from surface EMG recordings," *Journal of Electromyography and Kinesiology*, vol. 15, no. 3, pp. 310–315, Jun. 2005. DOI: 10.1016/j.jelekin.2004.10.001.

[39] A. E. Mendrela, J. Cho, J. A. Fredenburg, V. Nagaraj, T. I. Netoff, M. P. Flynn, and E. Yoon, "A Bidirectional Neural Interface Circuit with Active Stimulation Artifact Cancellation and Cross-Channel Common-Mode Noise Suppression," *IEEE Journal of Solid-State Circuits*, vol. 51, no. 4, pp. 955–965, Apr. 2016. DOI: 10.1109/JSSC.2015.2506651.

[40] R. Grieve, P. A. Parker, B. Hudgins, and K. Englehart, "Nonlinear adaptive filtering of stimulus artifact," *IEEE Transactions on Biomedical Engineering*, vol. 47, no. 3, pp. 389–395, 2000. DOI: 10.1109/10.827307.

[41] K. Zeng, D. Chen, G. Ouyang, L. Wang, X. Liu, and X. Li, "An EEMD-ICA Approach to Enhancing Artifact Rejection for Noisy Multivariate Neural Data," *IEEE Transactions on Neural Systems and Rehabilitation Engineering*, vol. 24, no. 6, pp. 630–638, Jun. 2016. DOI: 10.1109/TNSRE.2015.2496334.

[42] W. De Clercq, A. Vergult, B. Vanrumste, W. Van Paesschen, and S. Van Huffel, "Canonical correlation analysis applied to remove muscle artifacts from the electroencephalogram," *IEEE Transactions on Biomedical Engineering*, vol. 53, no. 12, pp. 2583–2587, Dec. 2006. DOI: 10.1109/TBME.2006.879459.

[43] H. Liang and Z. Lin, "Stimulus artifact cancellation in the serosal recordings of gastric myoelectric activity using wavelet transform," *IEEE Transactions on Biomedical Engineering*, vol. 49, no. 7, pp. 681–688, 2002. DOI: 10.1109/TBME.2002.1010851.

[44] T. Al-ani, F. Cazettes, S. Palfi, and J. P. Lefaucheur, "Automatic removal of high-amplitude stimulus artefact from neuronal signal recorded in the subthalamic nucleus," *Journal of Neuroscience Methods*, vol. 198, no. 1, pp. 135–146, May 2011. DOI: 10.1016/j.jneumeth.2011.03.022.

[45] E. Mastinu, P. Doguet, Y. Botquin, B. Hakansson, and M. Ortiz-Catalan, "Embedded System for Prosthetic Control Using Implanted Neuromuscular Interfaces Accessed Via an Osseointegrated Implant," *IEEE Transactions on Biomedical Circuits and Systems*, vol. 11, no. 4, pp. 867–877, 2017. DOI: 10.1109/TBCAS.2017.2694710.

[46] I. Technologies, *RHS2116 Digital Electrophysiology Stimulator / Amplifier Chip*, 2018.

[47] J. Maier, A. Naber, and M. Ortiz-Catalan, "Improved Prosthetic Control Based on Myoelectric Pattern Recognition via Wavelet-Based De-Noising," *IEEE Transactions on Neural Systems and Rehabilitation Engineering*, vol. 26, no. 2, pp. 506–514, Feb. 2018. DOI: 10.1109/TNSRE.2017.2771273.

[48] A. Naber, E. Mastinu, and M. Ortiz-Catalan, "Stationary Wavelet Processing and Data Imputing in Myoelectric Pattern Recognition on a Low-Cost Embedded System," *IEEE Transactions on Medical Robotics and Bionics*, vol. 1, no. 4, pp. 256–266, Nov. 2019. DOI: 10.1109/tmrb.2019.2949853.

[49] J. L. Hintze and R. D. Nelson, "Violin plots: A box plot-density trace synergism," *American Statistician*, vol. 52, no. 2, pp. 181–184, 1998. DOI: 10.1080/00031305.1998.10480559.

[50] B. Bechtold, "bastibe/Violinplot-Matlab: A Good Starting Point," Feb. 2021. DOI: 10.5281/ZENODO.4559847.

[51] H. B. Mann and D. R. Whitney, "On a Test of Whether one of Two Random Variables is Stochastically Larger than the Other," *The Annals of Mathematical Statistics*, vol. 18, no. 1, pp. 50–60, Mar. 1947. DOI: 10.1214/aoms/1177730491.

[52] M. P. Fay and M. A. Proschan, "Wilcoxon-Mann-Whitney or T-test? on assumptions for hypothesis tests and multiple interpretations of decision rules," *Statistics Surveys*, vol. 4, pp. 1–39, 2010. DOI: 10.1214/09-SS051.

[53] R. A. Armstrong, *When to use the Bonferroni correction*, Sep. 2014. DOI: 10.1111/opo.12131.

[54] Sture Holm, "A Simple Sequentially Rejective Multiple Test Procedure," *Scandinavian Journal of Statistics*, vol. 6, no. 2, pp. 65–70, 1979.

[55] A. Middleton and M. Ortiz-Catalan, "Neuromusculoskeletal Arm Prostheses: Personal and Social Implications of Living With an Intimately Integrated Bionic Arm," *Frontiers in Neurorobotics*, vol. 14, p. 39, Jul. 2020. DOI: 10.3389/fnbot.2020.00039.

DEPARTMENT OF ELECTRICAL ENGINEERING
CHALMERS UNIVERSITY OF TECHNOLOGY
Gothenburg, Sweden 2021
www.chalmers.se

CHALMERS
UNIVERSITY OF TECHNOLOGY